Factors contributing to upscale convective growth in the Central Great Plains of the United States

by

Zachary Aaron Hiris

A thesis submitted to the graduate faculty

in partial fulfillment of the requirements for the degree of

MASTER OF SCIENCE

Major: Meteorology

Program of Study Committee:
William A. Gallus, Jr., Major Professor
Alex Gonzalez
Kristie Franz

The student author, whose presentation of the scholarship herein was approved by the program of study committee, is solely responsible for the content of this thesis. The Graduate College will ensure this thesis is globally accessible and will not permit alterations after a degree is conferred.

Iowa State University

Ames, Iowa

2020

TABLE OF CONTENTS

Page

LIST OF FIGURES

Page

LIST OF TABLES

Page

ACKNOWLEDGMENTS

I would like to thank my major professor, Dr. William Gallus, for his thoughtful guidance, flexibility, and useful discussion during the past two years. I would also like to thank committee members Dr. Alex Gonzalez and Dr. Kristie Franz, for their help and supportive comments in improving this thesis. The help of fellow graduate students Jon Thielen, Michael Garberoglio, Ezio Mauri, and many others, who have provided idea sharing and assistance with coding has been greatly appreciated.

ABSTRACT

During the warm season, convection is a frequent occurrence across the Great Plains of the United States. Depending on storm mode, severe convection can contain a variety of threats, including tornadoes, large hail, strong winds, and flash flooding. The latter two of these are most commonly associated with mesoscale convective systems (MCSs), which, despite general improvements in forecasting convection, remain difficult to predict. While numerical weather prediction models have improved in resolution as a result of increased computational resources, predicting MCSs and their evolution remains a pertinent challenge. Thus, a further understanding of the physical mechanisms responsible for the formation of MCSs is needed in order to better predict these storms in the future. To better predict this phenomena, this work focuses on both quasi-real-world simulations using the Weather Research and Forecasting model (WRF) and and idealized cloud model (CM1) to differentiate between synoptic-, meso-, and storm-scale characteristics of non-MCS and MCS producing events.

First, the WRF model was used to simulate a total of 30 events during the 2016 warm season, including 15 non-MCS and 15 MCS producing convective days. These 24-hour simulations utilized a 3km horizontal resolution, which is representative of the resolution of current operational convective allowing models. Each simulation was analyzed to determine the ability of the WRF to properly distinguish between non-MCS and MCS producing days using GFS analyses as its initial and boundary conditions. It was found that WRF was generally able to predict these events, though identification of more specific convective modes were not considered. Then, a variety of potential factors influencing upscale convective growth were examined in detail, including several cold pool related parameters and vertical wind shear.

Second, idealized simulations utilizing pre-convective environments of the WRF were completed in a cloud resolving model (CM1). Here, horizontal and vertical resolutions were less than 500m. The 3-d structures of the convective updrafts and cold pools were examined after modifying thermodynamic variables and wind profiles to test the sensitivity of upscale growth. It was found that changes to the overall wind profile did little to influence overall convective evolution. The edge of the cold pool was also not the primary source of lift for parcels reaching the convective updrafts, and evidence suggests that gravity waves behind the cold pool edge may be contributing additional lift. Furthermore, in experiments with shallow and deep stable layers, surface-based convection still developed. While results from the CM1 indicate that there is likely a balance between the thermodynamic and kinematic fields that encourages upscale growth, a more thorough investigation is needed to better understand the physical processes driving convective growth in the CM1.

CHAPTER 1. GENERAL INTRODUCTION

1.1 General Introduction

Warm season convection accounts for a large percentage of overall rainfall in the Great Plains (Fritsch et al. 1986). Convective patterns can range from broad, isolated coverage of short-lived, poorly organized convective cells to well organized Mesoscale Convective Systems (MCSs), which can have lengths greater than 100km and traverse several hundred kilometers over many hours during their lifecycle (e.g., Maddox 1980; Blanchard 1990). While each convective mode contributes precipitation, other hazards associated with convection, such as tornadoes, large hail, damaging wind gusts, or extreme rainfall, are typically associated with specific types of convection.

As one example, supercellular thunderstorms are far more likely to produce tornadoes compared to other storm modes (Thompson et al. 2003; Grams et al 2004; Duda and Gallus 2010; etc). Organized MCSs, including bow echoes, often produce widespread wind damage, even late at night, when a stable boundary layer typically limits the occurrence of damaging winds (e.g., Parker et al. 2020). Furthermore, during transitional periods between isolated convection and organized MCSs, there is potential for multiple severe hazards to occur at one time (e.g., tornadoes and flash flooding), further complicating effective communication of storm-related threats (Nielsen et al. 2015). Therefore, it is critical to understand the physical processes which are responsible for the upscale convective growth from isolated convection to MCSs.

General forecasts of convection have steadily improved in recent years, primarily due to the increase in computing resources and, as a result, an increase in resolution of numerical weather prediction models (e.g., Gallo et al. 2017). This includes convective allowing models (CAMs; Weisman et al. 1997), in which convection is resolved by the model itself (e.g., Fowle and

Roebber 2003; Done et al. 2004; Weisman et al. 2008; Weiss et al. 2008). This increase in resolution has allowed for better simulation of supercell structure (e.g., Schwartz et al. 2009) and squall lines (Bryan and Morrison 2012). Though simulation of structures of convection has improved as a result, forecasting convective initiation and upscale growth remains an area of relatively poor forecast skill.

Forecasting convective initiation is challenging in most forecast patterns. Surface-based convection develops at or very close to the surface itself. CAM forecasts of CI are generally good within regimes of strong synoptic-scale forcings (e.g., frontal boundaries; Szoke et al. 2004; Wilson and Roberts 2006). With a lack of identifiable synoptic scale features, convective initiation then becomes dependent on mesoscale to microscale boundaries, which are typically finer scale than what CAMs can resolve. Elevated convection (e.g., Horgan et al. 2007; Corfidi et al. 2008), where convection initiates above the surface, is much harder to predict, and is often extremely sensitive to low-level temperature and moisture profiles aloft, where little to no observational data exists (Peters and Schumacher, 2016) .

Upscale convective growth is also a poorly understood phenomena, with little previous literature focusing on this aspect. Recent studies have indicated the upscale growth phase of MCSs is the least understood and poorly forecast portion of its convective lifecycle (Thielen and Gallus 2019). Like forecasts of convective initiation, upscale growth is likely significantly influenced by small changes in the ambient environment, including small differences in terrain height and planetary boundary layer temperature and moisture (Schumacher 2015).

One potential theory of how upscale growth occurs relates to convectively generated cold pools. As discussed further in Chapters 2 and 3, cold pools are generated as a result of latent cooling that occurs in storm's downdraft region (e.g., Droegemeier and Wilhemson 1985;

Weisman 1992; Mallinson and Lasher-Trapp 2019; Borque et al. 2020). As cold air accumulates at the surface and grows in depth, it can serve as a source for additional lift within the lowest few kilometers of the atmosphere. The resulting temperature gradient can create a strong, propagating density current, where the leading edge of the cold pool acts as a source of lift, especially if in balance with low-level shear (e.g. Rotunno et al. 1988; Weisman and Rotunno 2004). If the amount of lift generated by the cold pool can sufficiently lift a parcel to its level of free convection, this can began a positive feedback loop in which new convection develops, then repeatedly reinforces the strength of the cold pool via its new downdraft, thus organizing congealed convection along an expanding cold pool (Mulholland et al. 2019; Parker et al. 2020).

It is also possible that cold pools are influenced by mesoscale and synoptic scale features. James et al. (2005) found that cold pool strength was strongly correlated to changes in low-level thermodynamic profiles. Other work has theorized that deep layer vertical wind shear can influence the strength and orientation of the cold pool as a result of hydrometeor distribution in a storm's updraft and downdraft (Peters et al. 2017). Because the cold pool equation is directly related to the ambient environmental potential temperature, it is sensitive to spatiotemporal changes in the mesoscale environment to where convection propagates. Therefore, it is worthwhile to investigate and differentiate between both larger-scale and storm-scale environments of MCS- and non-MCS-producing days.

1.2 Research Questions and Thesis Organization

This thesis investigates the upscale convective growth phase by two distinct methods. First, the Weather Research and Forecasting model (WRF, Skamarock et al. 2019) is used to simulate 15 MCS and 15 non-MCS producing convective events over the Great Plains from 2016. We evaluate the model's ability to differentiate between MCS and non-MCS environments, specifically focusing on environmental conditions within the first few hours of

convective initiation. This includes calculating larger-scale parameters, including vertical wind shear, and storm-scale parameters such as the cold pool strength.

Then, an idealized cloud-resolving model (CM1, Bryan and Fritsch 2002; Bryan et al. 2003) is used to provide very high resolution simulations of convection based on environmental conditions provided by the WRF. To test the importance of deep layer shear and low level (in)stability, manually modified profiles are used in both MCS and non-MCS events.

This thesis follows the journal paper format. Chapter 1 contains a general introduction and describes the organization of the thesis. A detailed literature review of previous studies which focus on forecasting MCSs and other convection, cold pools, and idealized models is located in Chapter 2. Chapter 3 is a paper that will be submitted to Weather and Forecasting and contains the majority of the research completed. Chapter 4 contains a general conclusion section and potential options for future work in this area of focus. Finally, acknowledgements and references are located after Chapter 4.

CHAPTER 2. LITERATURE REVIEW

Forecasts of deep moist convection have been an area of study for the past several decades (e.g., Doswell 1987). Convection represents an important challenge for the Great Plains, accounting for a large percentage of warm season precipitation (e.g., Fritsch et al. 1986), but also producing severe weather (e.g. Duda and Gallus 2010; Grams et al. 2012, Smith et al. 2012). Given the extensive hazards associated with convection and different convective modes that occur in the Plains, there is a clear need for continued improvements in our understanding of deep moist convection and convective modes.

In recent years, general increases in predictability have been observed, largely as a result of increased resolution in numerical weather prediction models which permit deep convection to form in the absence of a convective parameterization scheme (CAMS, Weisman et al. 1997). Fowle and Roebber (2003) found forecasts of general convective mode and precipitation were improved using a mesoscale model at 6km resolution in quasi-real-world simulations. Others have also noted improved forecasts of convective mode (e.g., Done et al. 2004; Weisman et al. 2008; Weiss et al. 2008, etc.), convective structures (Schwartz et al. 2009), and precipitation forecasts (Clark et al. 2009). More recently, the use of high-resolution CAM ensembles has been found to provide useful uncertainty guidance (Clark et al. 2012; Guyer and Jirak 2014; Gallo et al. 2017; etc.). However, explorations into even finer-resolution (~1km) have shown mixed results. Notably, Thielen and Gallus (2019) found no statistical improvement in convective morphology classifications between 3km and 1km resolution forecasts. Squitieri and Gallus (2020) found that precipitation forecasts improved by increasing horizontal grid spacing from 3km to 1km, but propagation speeds of MCSs were better aligned with observations at 3km.

Predictability of convective initiation and convective mode also show increased skill when assimilating additional data. Simulations of convective events during the Mesoscale Predictability Experiment (MPEX, Weisman et al. 2015) showed that incorporating additional radiosondes allowed for improved forecasts of convective initiation (Coniglio et al. 2016; Hitchcock et al. 2016). At cloud-permitting resolutions, which are typical in idealized models, increases to resolution generally result in more accurately resolved convective features. In a squall line study, Bryan and Morrison (2012) found that structures of squall lines were much better represented by 250m resolution. Additionally, their study also notes much better representation of distributions of radar reflectivity and cold pool properties at a finer resolution.

Although there have been general improvements to forecasts of convection, there are still important mesoscale and storm-scale processes which remain poorly understood. In particular, the *upscale convective growth* (UCG) phase of the convective life cycle remains one of the more challenging aspects of forecasting convection. The UCG phase represents a transition from isolated, cellular convection to larger, organized, mesoscale convective systems. While cellular convection is more typically associated with tornadoes and large hail, MCSs often are more likely to produce wind damage and flash flooding (Doswell et al. 2005; Smith et al. 2012; Thompson et al. 2012; etc.). During the UCG phase, a combination of these impacts (e.g., tornadoes and flash flooding) can be observed simultaneously, making the UCG phase particularly important to message (Nielsen et al. 2015). Schumacher (2015) presents an example of the “dual-hazard” threat that can occur during UCG, in which numerical models poorly handled the transition from a supercell to a slow-moving, flash-flooding producing MCS. Hawblitzel et al. (2007) observed that small perturbations in temperature and wind led to significant changes in evolution of a strong mesoscale convective vortex. Thielen and Gallus

(2019) also noted the UCG phase was most often associated with the poorest skill in both 1km and 3km resolution simulations.

A variety of studies have begun to investigate synoptic and mesoscale characteristics commonly associated with UCG and MCSs. Jirak and Cotton (2007) detail a large database of MCS and non-MCS producing convection, finding that low-level temperature advection, 0-3km vertical wind shear, and static stability were the most important factors to producing MCSs. Coniglio et al. (2010; 2011) found steep low-level lapse rates, high precipitable water, and large amounts of convective available potential energy (CAPE) typically favor rapid UCG, especially if these ingredients are co-located at the nose of a low-level jet. Dial et al. (2010) note that for convection initiating along a boundary (e.g., a frontal boundary), UCG was more likely to occur if deep-layer wind shear was oriented parallel to the front, with similar results found by Duda and Gallus (2013). Peters and Schumacher (2015) developed composites of quasi-stationary, extreme rainfall producing MCSs, which featured convection developing at the terminus of a LLJ, strong synoptic scale warm air advection (WAA), and elevated instability.

While it is likely that synoptic scale variables play an important role in UCG, it is likely that storm-scale factors play an equally large or larger role. Mulholland et al. (2019) found that interactions between a topography and storm-scale features influenced UCG potential as a result of cold pool blocking. Recent idealized simulations from Parker (2018) and Parker et al. (2020) suggest that even in the absence of synoptic scale boundaries, convection can be self-organizing, largely due to the effects of cold pools and internally generated bores and gravity waves.

The convectively generated cold pool - a region of latently cooled air associated with convectively generated downdrafts - is perhaps the most classic example of a contributor to MCS maintenance (Droegemeier and Wilhelmson 1985; Rotunno et al. 1988; Weisman 1992). In

RKW theory (e.g., Rotunno et al. 1988), a balance between a convective cold pool and low-level vertical wind shear leads to a vorticity balance that promotes the formation of new updrafts, where the tilt of the updraft is determined by the ratios of cold pool and wind shear (see also Weisman and Rotunno, 2004). Several idealized simulations have confirmed that this relationship generally holds true (e.g., James et al. 2005, 2006; Bryan and Morrison 2012), though this is largely useful for predictability of MCS maintenance. Moreover, a recent study found that all MCSs observed during the recent Plains Elevated Convection at Night (PECAN, Geerts et al. 2017) featured at least a weak cold pool at the surface, despite a stable boundary layer (Hitchcock et al. 2019).

The cold pool itself is sensitive to a variety of environmental and storm-scale variables. James et al. (2005, 2006) note significant differences in cold pool strength as a result of small changes low and mid-level moisture. Peters and Schumacher (2016) found that MCS evolution is significantly different when evaporation in a model is turned off, suggesting that a combination of storm-scale cold pools and large scale factors such as WAA are important in developing new convection. Other studies by Peters and Schumacher (2016) and Peters et al. (2017) note that low-level moisture differences can significantly impact the size, location, and strength of MCSs. Furthermore, recent studies have also found that increases in low and mid-level shear favor wider updrafts, which in turn lead to stronger and wider cold pools (e.g., Marison and Trapp 2019). Cold pools are also likely influenced by hydrometeor distributions, and thus, microphysics parameterizations (Adams-Selin et al. 2013; Peters et al. 2017; Mallison and Lasher-Trapp 2019; Borque et al. 2020; etc.).

As mentioned previously, the cold pool is not the only potential storm-scale driven factor which may influence upscale growth. Both gravity waves (e.g., McAnelly et al. 1997; Adams-

Selin and Johnson 2013) and bores (e.g., Parker 2018; Haghi et al. 2019) have been shown to provide sufficient lifting to adequately generate new convection downstream, even in the absence of cold pools. Bores and gravity waves are more likely to develop and initiate convection when there is low-level stability (e.g., Marsham et al. 2011; Parsons et al. 2019, etc.). Several PECAN case studies have noted the importance of bores and gravity waves in maintaining convection. Gasmick et al. (2018) found that a nocturnal MCS was maintained by a combination of cold pools and bore-like boundaries. Zhang et al. (2020) noted a considerable amount of convective initiation (CI) was a result of a propagating bore ahead of the pre-existing convection. Many other studies focus on the impact of bores on nocturnal MCSs (Bodine and Rasmussen 2017; Chasteen et al. 2019; Haghi et al. 2019; Loveless et al. 2019), though little of this work explores how important of a role this places in the UCG phase. Though this is a small sample size of studies, it is worth noting that these studies are relatively recent, and highlight a need for further analysis of simulated UCG and the factors which influence UCG potential.

CHAPTER 3. FACTORS THAT CONTRIBUTE TO UPSCALE CONVECTIVE GROWTH IN THE CENTRAL GREAT PLAINS

A paper to be submitted to *Weather and Forecasting*

Zachary A. Hiris and William A. Gallus, Jr.

3.1 Abstract

Upscale convective growth remains a poorly understood aspect of convective evolution, and is often a period where numerical weather prediction models poorly depict convective structure and morphology. To better understand physical mechanisms which encourage upscale growth, a total of 30 warm season convective events from 2016 are simulated using the Weather Research and Forecasting (WRF) model to identify differences in upscale growth and non-upscale growth environments. Then, several Bryan Cloud Model (CM1) sensitivity tests are completed testing a variety of thermodynamic environments and wind profiles to examine the impact on upscale growth.

It was found that there are few differences in cold pool strength between upscale growth and non-upscale growth events in the WRF, but statistically significant differences exist in deep layer shear magnitudes. In the CM1, all sensitivity tests of the upscale growth event formed an MCS, while all non-upscale growth tests sustained a single convective cell for 1-6 hours. CM1 sensitivity tests also suggested that the organization and orientation of the convectively-generated cold pool and other internal factors including gravity waves also likely influence upscale growth, in addition to deep-layer shear.

3.2 Introduction

The *upscale convective growth* (hereafter UCG) phase, which represents the transition from isolated convective cells to organized mesoscale convective systems (MCSs, e.g., Blanchard 1990), remains a difficult forecasting challenge. A better understanding of

mechanisms which drive UCG is critical, as the transition period between cellular convection and MCSs is also associated with a transition in primary severe convective hazards. Discrete modes, including supercells, are much more frequently associated with large hail and tornadoes, while MCSs are more commonly associated with damaging winds and flash flooding (Thompson et al. 2003; Doswell et al. 2005; Smith et al. 2012; Thompson et al. 2012; etc.). During the UCG phase, an overlapping period of these hazards is possible, which creates challenges for properly messaging safety procedures (Nielsen et al. 2015).

Despite general improvements to forecasting convective initiation and morphology (e.g., Clark et al. 2009; Schwartz et al. 2009; among many others), less progress has been noted in ingredients based forecasts of upscale growth. Jirak and Cotton (2007) found that low-level temperature advection, low-level (0-3km) wind shear, and low static stability were the most important factors in producing rapid upscale convective growth. Coniglio et al. (2010; 2011) found steep low-level lapse rates, high precipitable water, and large amounts of CAPE also contribute to UCG. Dial et al. (2010) noted that convection initiating along a boundary was more likely to grow upscale if the deep-layer wind shear vector was oriented parallel to the front (see also Duda and Gallus 2013). Many of these components were also found to be important in composites of extreme rain-fall producing MCSs (Peters and Schumacher 2015).

Numerical simulations at convective allowing resolutions (e.g., CAMs; see Weisman et al. 1997) have seen similarly poor results when forecasting UCG. Using CAMs as a tool for predicting convective mode has been well documented in the last several years (e.g., Fowle and Roebber 2003; Done et al. 2004; Weisman et al. 2008; Weiss et al. 2008; Clark et al. 2012; Guyer and Jirak 2014; Gallo et al. 2017, etc). However, studies have continued to note poor performance during the UCG phase. Hawblitzel et al. (2007) observed wildly varying solutions

due to small perturbations of temperature and moisture. Schumacher (2015) noted poor skill in various WRF simulations of the 31 May - 1 June 2013 supercell to MCS transition. Theilen and Gallus (2019) found no statistically significant improvements in convective morphology forecasts between 3- and 1km WRF simulations, despite an increased occurrence of linear events in the climatology that agreed better with the observed climatology, and specifically note that the UCG phase was often associated with the poorest model skill.

Questions also arise from the impact of aforementioned synoptic-scale external forcings compared to storm scale forcings (e.g., cold pools and/or other density currents). Downdrafts, as a result of latent cooling and precipitation loading, can result in the formation of convectively generated cold pools (e.g., Droegemeier and Wilhelmson 1985; Weisman 1992). In certain regimes, cold pools can interact with a favorable low-level wind shear profile to generate new convective cells for MCS maintenance (Rotunno et al. 1988; commonly referred to as RKW theory). Additionally, convectively generated cold pools can also initiate gravity waves and bores (McAnelly et al. 1997; Bryan and Rotunno 2014; Parker 2018). A recent study from Peters and Schumacher (2016) found that in a single MCS, both internal and external forcings may contribute to the development of new convective cells along different parts of the MCS (in addition to temporal changes). Other recent work from Mulholland et al. (2019) suggests that terrain-influenced cold pool blocking (and therefore a strengthening of the cold pool via cold air accumulation) contributed significantly to UCG in a case study of a South American MCS. Further work from Parker (2018) and Parker et al. (2020) suggests that UCG can be entirely internally driven by both convectively generated cold pools and bores.

Cold pools are influenced significantly by parent storm characteristics. Increases to low- and mid-level shear have been shown to favor larger updrafts, which in turn lead to stronger and

wider cold pools (e.g., Marion and Trapp 2019). Cold pools are also sensitive to hydrometeor distributions, and thus, would likely be influenced by microphysical parameterizations (Adams-Selin et al. 2013; Mallinson and Lasher-Trapp 2019; Borque et al. 2020). Other work has suggested that deep layer shear also strongly influences these hydrometeor distributions, and thus, the development of the cold pool on the rear or forward flank of a convective cell (Peters et al. 2017). Furthermore, all observed MCSs during the recent Plains Elevated Convection at Night (PECAN; Geerts et al. 2017) contained at least a weak surface cold pool, even when a stable boundary layer was also observed (Hitchcock et al. 2019). Therefore, it appears likely that cold pool processes play a role in the UCG phase of MCSs containing both surface based and elevated convection.

Thus, there remains a need to better understand the UCG phase of convective development. In particular, this study investigates UCG using two distinct approaches. First, the Weather Research and Forecasting Advanced Research WRF v4.0 (WRF-ARW, Skamarock et al. 2019) is used to simulate several MCS and non-MCS cases, focusing on differences in both external and internal forcings among the cases. Secondly, an idealized, cloud-resolving model (CM1; Bryan and Fritsch 2002) is used to simulate an MCS case under a variety of thermodynamic and kinematic regimes in an attempt to replicate the self-organizational processes described by Parker et al. (2020). The manuscript here is structured in the following manner: section 2 provides a detailed description of the data and methods of this study, section 3 provides results from various real-world and idealized numerical simulations. General summary and conclusions are provided in section 4.

3.3 Data and Methodology

3.2.a Selection of Cases

A total of *n=30* cases were manually selected from the months of May - August 2016. This includes 15 cases in which convection developed but did not grow upscale (hereafter non-UCG cases) and 15 "quasi-pristine" upscale growth cases (hereafter UCG cases). "Quasi-pristine" upscale growth here is defined as convection which develops and grows upscale into an MCS in an unperturbed environment (i.e., an absence of significant downstream convection). To identify these events, radar data from each day were examined using the UCAR Image Archive browser (https://www2.mmm.ucar.edu/imagearchive) over the Central Great Plains Sector, with a focus on convective development and subsequent upscale growth to occur between 1600-0600 UTC. Days which featured significant downstream convection and/or multiple segments with various levels of organization, or did not contain any convection were excluded. Events which featured upscale growth outside the specified time period were also excluded.

Cases were identified based on criteria described by James et al. (2005) and Duda and Gallus (2010). An event was classified as an MCS if the convective region (reflectivity >40 dBZ) covered a sufficiently large area (100 km in length), persisted for at least two hours, and had a length:width ratio of at least 3:1. This incorporates many of the traditional morphologies such as trailing stratiform or bow echoes, though here the specific subtype of MCS is not identified, unlike in Gallus et al. (2008) or other recent studies of morphology (Thielen and Gallus 2019). Instead, the focus in this work is to contrast events where MCSs formed (UCG) versus those where they did not (non-UCG), though future work should incorporate a further analysis of convective morphology. Non-MCS cases exhibited no upscale growth and did not meet the criteria described above. A full list of all cases used in this study is provided in Table 1.

3.2.b WRF Simulation Setup

The WRF-ARW version 4.0 was utilized using two large, coarse resolution outer domains (27 km, 9 km) and a smaller, 3 km inner domain (Fig. 1). Two-way feedback was enabled between all domains. The model domain was unchanged for all event simulations. All simulations used 0.5° GFS analysis data (NOAA-NCEI 2019) for their initial conditions and lateral boundary conditions. A total of 50 vertical layers was used, as in Squitieri and Gallus (2016, 2020). The Morrison double-moment physics scheme (Morrison et al. 2009) was used for all events, as other schemes often failed to produce realistic depictions of stratiform precipitation (not shown, this was also observed by Thielen and Gallus 2019). A full description of the model setup is found in Table 2.

In addition to the 30 simulations using the Morrison microphysics scheme, this study also tests the impact of three other microphysics schemes on the development of convective cold pools for one MCS case (13 July 2016) and one non-MCS case (08 August 2016). For these randomly selected cases, additional WRF simulations were completed using the Thompson (Thompson et al. 2008), WSM6 (Hong and Lim 2006), and NSSL 2-moment schemes (Mansell et al. 2010). We compare differences of convective development and evolution, along with differences of cold pool strength, in section 3.4b.

3.2.c Idealized CM1 Simulations

The Bryan Cloud Model (CM1, Bryan and Fritsch 2002; Bryan et al. 2003), version 19.7 was used for idealized simulations of convection. The CM1 was run in the present study with a much higher resolution than the WRF, allowing for investigation of the impact of internal factors on UCG (or lack thereof). As the CM1 requires fewer parameterizations, the model is much less computationally expensive. The model was horizontally homogeneous, with the base state

described by an input model sounding from the aforementioned WRF simulations, which is shown in (Fig. 2). A basic description of the model setup is also provided in Table 3.

To initialize convection in the CM1, a line of four evenly spaced warm bubbles was placed in the center of the domain. These bubbles were centered at a depth of 1.7 km, with a horizontal radius of 10 km, a vertical radius of 1.7 km, and a maximum potential temperature perturbation of 3 K. Sensitivity tests between different initialization methods (not shown) suggested that impacts to overall convective evolution were minor, which was also implied by Parker (2018) and Parker et al. (2020).

In order to understand the importance of the base-state thermodynamic and kinematic profiles, four primary tests are conducted. First, a control run (hereafter CTRL) was performed by simply using the base state sounding described previously. Second, an isothermal stable layer was introduced to approximately the lowest 750 m of the input sounding (hereafter SBL750) and 250 m (SBL250). Third, the wind profiles of the UCG and non-UCG case are simply flipped (WINDR). For all tests, a passive tracer was initialized in the lowest 500 m of the model, with a second tracer added between 4-5 km. This allowed for examination of updraft and downdraft origins. Importantly, this also allowed for investigation of how the surface stable layer impacts downdraft propagation to the surface and the possible transition to surface based convection.

3.2.d Cold Pool Parameters

To quantify the strength and structure of the 3-dimensional cold pools of MCS and non-MCS cases, several cold pool parameters were calculated, following Squitieri and Gallus (2020). The cold pool parameter (*C*, Rotunno et al. 1988; Weisman and Rotunno 2004; James et al. 2005; etc.) – which represents a theoretical speed of a two-dimensional gravity current (e.g., the cold pool), perturbation potential temperature (θ'), cold pool depth, and buoyancy fields were obtained. The cold pool parameter *C* is defined to be representative of the propagation of the

density current (in ms^{-1}). A generalized equation of *C* from Weisman (1992) and James et al. (2005) is given by:

$$C^2 = \int_0^H (-B)\, dz \tag{1}$$

where *B* is buoyancy, and *H* is the top of the cold pool. Buoyancy is defined as:

$$B \equiv g\left[\frac{\theta'}{\bar{\theta}} + 0.61(q_v - \overline{q_v}) - q_c - q_r\right] \tag{2}$$

In (2), g is gravity and $\bar{\theta}$ and θ' are ambient mean potential temperature and perturbation potential temperature, respectively. Water vapor, cloud water, and rain water mixing ratios are represented by q_v, q_c, and q_r, where $\overline{q_v}$ represents the ambient mean vapor mixing ratio.

In the CM1, calculations of the cold pool, and the variables described in (2) are easily derived from the base state condition, and *C*, *B*, and θ' are explicitly output by the model itself. However, in WRF, the ambient environment is heterogeneous, which must be taken into account. The methods of Squitieri and Gallus (2020) are utilized heavily for WRF calculations of the cold pool. To provide a good representation of *only* the convectively generated cold pools of interest, WRF data is subsetted to small (typically 4°x3°) subdomains in which all cold pool calculations are restricted. This eliminated the potential for other convective environments to be included when calculating ambient environmental temperature and moisture, and also eliminated the possibility of other convection outside the focus area to skew cold pool calculations. To evaluate possible differences in cold pools of UCG and non-UCG cases, several statistical tests are performed at each of the first five hours following convective development. These tests were performed across the entire distribution of variables, and also on grid points exceeding specific percentile thresholds. Because of the relatively small number of values across some percentiles,

bootstrapped *t*-tests were employed, with a resampling of $n = 1000$ on both the cold pool parameter *C* and various vertical wind shear magnitudes.

3.4 Results

3.4.a WRF Predictability of UCG

Though the primary focus of this paper was to evaluate physical differences between environments that feature UCG and those that do not, it was first worthwhile to evaluate whether the WRF is capable of consistently predicting broad UCG and non-UCG environments in this specific WRF setup. To evaluate general predictability, a simple scoring method was employed here. If a WRF simulation properly predicted an MCS (or non-MCS), the particular case was given a score of 1. Incorrect convective evolution, or a lack of sustained convective development, was given a score of 0. Importantly, this method does not look to investigate specific morphology subsets (e.g., Gallus et al. 2008; Duda and Gallus 2010; Thielen and Gallus 2019, etc.), and instead only evaluates the general predictability of UCG. Of the 30 total simulations, the WRF has a predictability rate of 0.8 (24 of 30 cases). A slight overprediction of UCG was observed, where four of the six incorrect forecasts were observed non-MCS events predicted as MCS events in the WRF.

3.4.b Simulated Cold Pool Strength

The strength and structure of convectively generated cold pools were evaluated within the first five hours of convective initiation in all cases, to investigate if cold pool strength could be correlated with UCG. Bootstrapped *t*-tests were performed on aggregated variables including the cold pool parameter *C*, and vertical wind shear magnitudes of all UCG and non-UCG cases. Cold pool strength was investigated as a whole, and was also subsetted into values exceeding different percentile thresholds, as done by Squitieri and Gallus (2020). For all hours, the two-tailed *t*-test was employed to determine if MCS-forming cold pools were significantly

stronger compared to those of non-MCS cases. The achieved level of significance (i.e., the *p* value) was calculated to determine statistical significance (Mendenhall and Sincich 2007; Squitieri and Gallus 2020).

Statistical tests were employed for the five hours following convective initiation (here, this was the first timestep when lowest model reflectivity becomes greater than 45dBZ), and statistical significance was computed for areas consisting of the entire cold pool (i.e., 0th percentile), >25th, median (>50th), >75th, and >99th percentiles. The cold pools of all UCG cases were aggregated, as well as those of non-UCG cases. These thresholds were subjectively chosen to better understand if there are large differences in overall cold pool structure, and/or if there are large differences between the two event types in the strongest portions of the cold pool.

In the first hour after convective initiation, cold pools were significantly ($p < 0.01$) stronger across the 25th, 50th, 75th, and 99th percentiles of UCG events (Fig. 2a). The distribution of the total cold pool, however, was not statistically significant. Median cold pool (*C*) strength in UCG cases was 15.04 m s^{-1}, compared to 14.73 m s^{-1} in non-UCG cases. By the second hour, the cold pool in UCG cases weakens (median magnitudes 13.49 m s^{-1}), and UCG cold pools are either significantly weaker or of equal strength compared to non-UCG cases. A distinct bi-modal distribution was observed in UCG cold pools, which continues to be evident in the following hour (Fig. 2b). Though this bi-modal distribution was still evident three hours after CI, UCG cold pools became significantly stronger than in non-UCG cases across all thresholds, with median values of 18.83 m s^{-1} and 17.99 m s^{-1}, respectively. Interestingly, the bi-modal distribution of *C* in MCS cases was not evident four hours after convective initiation, but cold pools were again statistically weaker, or differences between UCG and non-UCG cases were

insignificant. This was also observed at five hours after convective initiation, with median *C* values of 22.33 m s^{-1} and 25.3 m s^{-1} in UCG and non-UCG cases, respectively (Fig. 3).

To test if cold pool distributions were affected by large, weakly negatively buoyant stratiform regions, only the significantly convective (>45 dBZ) regions of the cold pool were tested. When only accounting for the convective area cold pool, cold pools of UCG cases were significantly stronger across all percentile thresholds used in the first hour after CI. The median *C* magnitude in UCG convective areas was 16.18 m s^{-1}, compared to 13.5 m s^{-1} for non-UCG cases. However, there was still an observable bi-modal distribution to *C* in MCS cases in hours two and three as described above, with very little change in the differences in magnitude between UCG and non-UCG cases. Though others have noted the importance of terrain blocking for stronger cold pool development and subsequent UCG (e.g., Mulholland et al. 2019), in relatively flat or sloping terrain in the central Great Plains, overall cold pool strength shows no differences in UCG and non-UCG cases.

3.4.c. Vertical Wind Shear

Shear in low-levels, mid-levels, and through a deep layer were all investigated through similar methods as described in the previous subsection. Specifically, 0-1 km, 0-2.5 km, 0-6 km, and 2-5 km shear were examined for the same five hour period as the cold pool magnitudes.

Deep layer shear (0-6 km) was much stronger in magnitude in cases which featured UCG compared to non-UCG events. In the first hour after CI, median 0-6 km shear was almost 10 m s^{-1} stronger in UCG cases (~22 m s^{-1} vs. ~14.5 m s^{-1}), which was statistically significant at all of the aforementioned percentile thresholds (Fig. 4). Deep layer shear magnitudes remained relatively constant over time, with median UCG (non-UCG) magnitudes increasing to 26.4 (15.7) m s^{-1} by the fifth hour (Fig. 5). Notably, UCG cases had statistically significantly stronger deep layer shear at all hours and percentile thresholds.

Initially, 0-1 km shear was also significantly stronger in UCG cases compared to non-UCG cases, with median magnitudes for UCG (non-UCG) cases of 9.1 (5.5) m s^{-1} an hour after convective initiation (Fig. 6). This increased in both UCG (non-UCG) cases to 10.3 (7.2) m s^{-1} an hour later, with differences still statistically significant. By hours four and five, non-MCS cases were located in environments with significantly larger 0-1 km shear. Similarly, 0-2.5 km shear displayed an identical trend, where UCG environments initially had larger shear magnitudes than non-UCG (Fig. 7). By hours three through five, differences in 0-2.5 km shear magnitudes revealed no clear tendencies, with many percentile thresholds showing insignificant differences (not shown).

3.4.d. WRF Microphysics Sensitivities to UCG

Four different microphysics parameterizations were tested on a random upscale growth and a non-upscale growth case in order to test the sensitivity of UCG to variations in microphysics scheme sensitivities. In both the UCG and non-UCG event, all four of the microphysics schemes tested produced similar convective evolution (Figs. 8-9). In general, the WSM6 produced the strongest cold pools of the four schemes, and produced gust fronts earlier than any other scheme in both the UCG and non-UCG events. In both event types, convective initiation was not impacted by microphysics choice, and occurred within a 30 minute window between all microphysics schemes (not shown).

In the UCG event, the WSM6 produced a much stronger and deeper cold pool than present with the other three schemes, with the other schemes all relatively similar to one another. Median C values peak five hours after convective initiation at just over 30 m s^{-1}, θ' values at -11 K, and cold pool depths at over 2500 m. These were much stronger than any of the other three microphysics schemes, whose median C values at peak cold pool strength ranged from 23-27 m s^{-1}, while θ' values never exceed -10 K (Fig. 10). This could explain why the WSM6 weakened

the system dramatically approximately 90 minutes later, when a clear gust front is noted in simulated lowest model level reflectivity. Other microphysics schemes did show evidence of a gust front, though it appeared much later, and expansive convection still appeared behind the gust front, unlike in the WSM6 (Fig. 9). Given that other microphysics schemes all produced similar magnitudes of C, θ', and cold pool depth, it appears that the early dissipation of convection was strongly related to the stronger cold pools the WSM6 generates.

In the non-UCG event, there are less notable differences in median and mean cold pool variables (Fig. 11a) among the four schemes. Each of the four microphysics schemes at one point in time had the largest mean and median magnitude of C, which was relatively unsurprising given that cellular convection is much more sensitive to pulses in downdraft strength, and that individual cells develop/decay differently with each microphysics option. Interestingly, there were clear differences in mean/median surface potential temperature perturbation (θ') and cold pool depth among the schemes. The NSSL 2-moment scheme produced a higher cold pool depth (generally >200 m deeper) than any other scheme, which was not the case for the UCG event. The WSM6 produced the largest magnitude of θ' at nearly all timesteps, with a peak median θ' of nearly -11 K, which was 2-3 K colder than with any other microphysics scheme (Fig. 11b). There was also evidence of several gust fronts in the WSM6 simulated radar reflectivity field (Figs. 12-13), suggesting that the overaggressive cold pool generation of the WSM6 led to unrealistic storm evolution. The Morrison, Thompson, and NSSL 2-moment schemes all produced relatively similar distributions of C and θ', which, since synoptic-scale details were similar, led to generally consistent convective evolution.

3.4.e. CM1 Simulations

Both a UCG and a non-UCG case were simulated with the CM1 using WRF soundings (Fig. 14a-b) as input to investigate the impacts of internal factors on convective behavior. Both CTRL experiments in the CM1 were able to capture the general morphology and storm lifecycle relatively well. In the UCG case, a large, slightly bowing, MCS formed within five hours of convective initiation, with nearly identical 2-d convective structure compared to both the WRF simulation and observations (Fig. 15). The CTRL sounding (Fig. 14a) was favorable for surface-based convection, and updrafts contained 0-500 m tracer through the duration of the simulation, and a strong cold pool developed early on in the simulations (Fig. 16).

In the 250 m deep stable layer (SBL250) experiment, the UCG case still grew upscale, though MCS progression was slightly slower than in the CTRL simulation (Fig. 17). Despite surface temperatures on the order of ~3 K lower than in the CTRL, the SBL250 experiment still developed a surface-based cold pool within an hour of convective initiation. In the deep, isothermal environment in the 750 m deep stable layer (SBL750) simulation, MCS growth was much more delayed. The initial four cells congealed into a single cell quickly, and gradually grew into a smaller system that almost but does not quite meet the size requirements for an MCS. Initially surface potential temperature perturbations were positive, but still a cold pool formed midway through the simulation. When the cold pool formed, surface-layer tracers were contained in the updraft, strongly indicating that surface or near-surface based convection still can occur even in the presence of the deep surface stable layer (Fig. 18).

In the UCG WINDR experiment, despite the use of the non-UCG wind profile, extensive convective development still occurred and is sustained through the duration of the simulation. There is far more “spurious” convection compared to that of the CTRL, SBL250, and SBL750.

However, an MCS still developed, and many of the reflectivity characteristics are comparable to both the simulated CTRL and observed reflectivity from the event (Fig. 19).

The CTRL non-UCG case sustained one cell for over an hour, before it eventually dissipated. This is generally a shorter storm lifecycle compared to what was both observed and simulated in the WRF (Fig. 20), but importantly the CM1 captured the lack of sustained convection and lack of upscale growth, despite a favorable thermodynamic profile and essentially no convective inhibition in the base state sounding. Convection was actually sustained much longer in the non-UCG SBL250 experiment compared to CTRL. A single cell was sustained for the entire duration of the event, and a broad cold pool still develops (Fig. 21a-b). The SBL750 experiment was similar to the CTRL, where convective cells dissipated within a few hours of the simulation (Fig. 21c). In the WINDR experiment, convection still failed to be sustained through the duration of the simulation, and dissipated quicker than in any other simulation (Fig. 21d). It is unclear why only the SBL250 simulation maintained convection through the duration of the simulation. Between each experiment, differences of CAPE and CIN are small (<10 J kg^{-1} and <2.5 J kg^{-1}, respectively), which strongly suggests that subtle thermodynamic changes have large impacts on convective evolution.

3.5 Summary and Conclusions

This work provides the first extensive documentation of model-simulated 3-D cold pools across a large number of both UCG and non-UCG events. While previous studies have focused on single events (e.g., Mulholland et al. 2019) and cold pools at MCS maturity (e.g., Squitieri and Gallus 2020), the authors here are unaware of any studies which thoroughly investigate both synoptic- and storm-scale variables thought to influence the upscale growth potential of deep moist convection, through both convection-allowing WRF experiments, and cloud resolving CM1 experiments. To accomplish this, a total of 15 UCG and 15 non-UCG convective events

from the 2016 warm season were simulated using the WRF. The model domain covered a large portion of the Central Great Plains, and analysis of the WRF simulations revealed that general predictions of whether convection will grow upscale or not are good, with a success rate of 80% (24 of 30 cases). The WRF in its specific setup here (Table 2) showed a slight overprediction of UCG events, with 4 of the 6 incorrect forecasts showing UCG in cases where observations did not.

From all 30 WRF simulations used, several cold pool variables were calculated, including the cold pool parameter *C*, perturbation potential temperature θ', and cold pool depth, with these variables aggregated over event type, and computed at a frequency of one hour. Several statistical tests were employed in order to evaluate differences in cold pool strength between UCG and non-UCG events during the first five hours following convective initiation. It was found that cold pools are statistically stronger in UCG events one hour after CI, with median values of *C* roughly 1 m s^{-1} greater in UCG events. However, UCG event cold pools are weaker or of similar magnitude in the following hour, and no consistent trend in cold pool strength is observed through the remainder of the five hour period.

In order to ensure that the aforementioned (in)significance of cold pool strength was not impacted by a potentially large area of stratiform region (typically less negatively buoyant, and thus a smaller magnitude of *C*) contributing to a decrease in median cold pool strength in UCG events, a statistical evaluation of only the strongly convective regions (>45 dBZ) was performed. Results here suggest that focusing only on the cold pool within convective regions does little to impact overall trends of cold pool strength in both UCG and non-UCG events. This suggests that cold pool strength is not a reliable predictor of UCG potential, and hints that other synoptic-, meso-, or storm-scale variables are likely the cause for UCG.

The importance of low-level, mid-level, and deep-layer shear was investigated using similar methods as described above. Importantly, deep-layer (0-6 km) wind shear was significantly stronger in UCG cases at all hours, with median magnitudes 5-10 m s^{-1} larger in UCG events at every hour tested. This strongly suggests that deep layer shear plays an important role in the UCG process, though an understanding of the direct impacts it has on convection is beyond the scope of the present study. Furthermore, low-level (0-1 km, 0-2.5 km) shear was significantly stronger in UCG events initially, though after a few hours shear was either weaker or insignificantly different from non-UCG events.

To determine the impact of the specific cloud microphysics parameterization scheme used in the WRF, three other microphysics schemes were tested on one randomly chosen UCG event and one non-UCG event. Generally, each of the four microphysics schemes produce similar convective patterns during the upscale growth phase of convective development. The WSM6 microphysics scheme produced the strongest cold pool in the UCG event, with C and θ' magnitudes approximately 5 m s^{-1} and 1 K greater, respectively, than the values from the other schemes. The WSM6 also produced a gust front before any other scheme, and dissipated convection quicker as a result. In the non-UCG event, there were no clear differences between the schemes in peak magnitudes of C, but the WSM6 again had much greater magnitudes of θ', that were up to 2-3 K cooler than with any other scheme. Despite differences in cold pool strength across the four schemes, each produced cellular convection that failed to grow upscale. This supports the idea that upscale growth is not necessarily dependent on cold pool strength, and thus is not strongly dependent on the choice of microphysics scheme. The idea that a cold pool could become too strong to support organized convection has been posed before, particularly from the application of RKW theory (Weisman and Rotunno 2004; James et al.

2005, 2006). While most studies have focused on the maintenance of a pre-existing MCS, the cold pool/shear balance described in RKW may also be applicable to the organization stages of an MCS as well.

Finally, in addition to the WRF investigation of upscale growth, thermodynamic and kinematic sensitivities were tested in several CM1 experiments. Using WRF sounding data for initialization, the CTRL runs of both a UCG and a non-UCG event produced accurate representations of convective mode (e.g., MCS or non-MCS). Accurate representations also occurred when a shallow stable layer (SBL250 experiments) was introduced, and to some extent, when a deeper stable layer was used. Flipping the wind profiles of the UCG and non-UCG events showed little impact on overall convective mode, suggesting that internal mechanisms are the driving force behind upscale growth. In all experiments, a surface cold pool develops and spreads laterally. This is supported by observational studies (Hitchcock et al. 2019), and recent work with CM1 in stable boundary layers (Parker et al. 2020). What is less clear is how the UCG WINDR and SBL250 experiments were able to still capture specific convective elements found in both observations, the CTRL, and WRF simulations of the event. While the WRF portion of this study strongly supports the idea that deep-layer shear is of particular importance, the results of the WINDR experiment suggest that there is clearly some unknown, *internal* factor which is critical during the UCG phase.

The upscale convective growth phase of deep moist convection remains poorly understood and forecast (e.g. Schumacher 2015; Mulholland et al. 2019), and represents an area of significant interest for operational forecasts of severe convection (e.g., Thompson et al. 2003; Duda and Gallus 2013; Nielsen et al. 2015). It is recommended that future work incorporate both WRF and CM1 in tandem, as done in the present study, to better discern what causes UCG in

heterogeneous and homogeneous environments. In particular, the internal drivers of UCG must be investigated in more detail to improve understanding of UCG in both surface-based and elevated convective regimes.

3.6 Acknowledgements

This research was supported primarily by National Science Foundation grant AGS1624947. The author would like to thank Jon Thielen for his extensive help in providing Python code used during various portions of this work, and Brian Squitieri for the original code used for calculating the cold pool. Comments provided by Matt Parker (NCST) were also quite useful for installing and troubleshooting the CM1. The author extends thanks to Dave Flory and Daryl Herzmann of Iowa State for their help in working with the Iowa State supercomputers, which were used extensively over the course of this work.

3.7 References

Adams-Selin, R. D., S. C. van den Heever, and R. H. Johnson, 2013: Sensitivity of bow-echo simulation to microphysical parameterizations. *Wea. Forecasting*, **28**, 1188-1209, https://doi.org/10.1175/waf-d-12-00108.1.

Blanchard, D. O., 1990: Mesoscale convective patterns of the Southern High Plains. *Bull. Amer. Meteor. Soc.*, **71**, 994-1005, https://doi.org/10.1175/1520-0477(1990)071%3C0994:mcpots%3E2.0.co;2.

Borque, P., S. W. Nesbitt, R. J. Trapp, S. Lasher-Trapp, and M. Oue, 2020: Observational study of the thermodynamics and morphological characteristics of a midlatitude continental cold pool event. *Mon. Wea. Rev.*, **148**, 719-737, https://doi.org/10.1175/mwr-d-19-0068.1.

Bryan, G. H., J. M. Fritsch, 2002: A benchmark simulation for moist nonhydrostatic numerical models. *Mon. Wea. Rev.*, **130**, 2917-2928, https://doi.org/10.1175/1520-0493(2002)130%3C2917:absfmn%3E2.0.co;2.

Bryan, G. H., J. C. Wyngaard, and J. Michael Fritsch, 2003: Resolution requirements for the simulation of deep moist convection. *Mon. Wea. Rev.*, **131**, 2394-2416, https://doi.org/10.1175/1520-0493(2003)131%3C2394:rrftso%3E2.0.co;2.

Bryan, G. H., and R. Rotunno, 2014: The optimal state for gravity currents in shear. *J. Atmos. Sci.*, **71**, 448-468, https://doi.org/10.1175/jas-d-13-0156.1.

Clark, A. J., W. A. Gallus, M. Xue, and F. Kong, 2009: A comparison of precipitation forecast skill between small convection-allowing and large convection-parameterizing ensembles. *Wea. Forecasting*, **24**, 1121-1140, https://doi.org/10.1175/2009waf2222222.1.

Clark, A. J., J. S. Kain, P. T. Marsh, J. Correia, M. Xue, and F. Kong, 2012: Forecasting tornado pathlengths using a three-dimensional object identification algorithm applied to convection-allowing forecasts. *Wea. Forecasting*, **27**, 1090-1113, https://doi.org/10.1175/waf-d-11-00147.1.

Coniglio, M. C., J. Y. Hwang, and D. J. Stensrud, 2010: Environmental factors in the upscale growth and longevity of MCSs derived from Rapid Update Cycle analyses. *Mon. Wea. Rev.*, **138**, 3514-3539, https://doi.org/10.1175/2010MWR3233.1.

Coniglio, M. C., S. F. Corfidi, and J. S. Kain, 2011: Environment and early evolution of the 8 May 2009 derecho-producing convective system. *Mon. Wea. Rev.*, **139**, 1083-1102, https://doi.org/10.1175/2010MWR3413.1.

Dial, G. L., J. P. Racy, and R. L. Thompson, 2010: Short-term convective mode evolution along synoptic boundaries. *Wea. Forecasting*, **25**, 1430-1446, https://doi.org/10.1175/2010waf2222315.1.

Done, J., C. A. Davis, and M. Weisman, 2004: The next generation of NWP: Explicit forecasts of convection using the weather research and forecasting (WRF) model. *Atmos. Sci. Lett.*, **5**, 110-117, https://doi.org/10.1002/asl.72.

Doswell, C. A., H. E. Brooks, and M. P. Kay, 2005: Climatological estimates of daily nontornadic severe thunderstorm probability for the United States. *Wea. Forecasting*, **20**, 577-595, https://doi.org/10.1175/waf866.1.

Droegemeier, K. K., and R. B. Wilhelmson, 1985: Three-dimensional numerical modeling of convection produced by interacting thunderstorm outflows. Part II: Variations in vertical wind shear. *J. Atmos. Sci*., **42**, https://doi.org/10.1175/1520-0469(1985)042%3C2404:tdnmoc%3E2.0.co;2.

Duda, J. D., and W. A. Gallus, 2010: Spring and summer Midwestern severe weather reports in supercells compared to other morphologies. *Wea. Forecasting*, **25**, 190-206, https://doi.org/10.1175/2009waf2222338.1.

Duda, J. D., and W. A. Gallus, 2013: The impact of large-scale forcing on skill of simulated convective initiation and upscale evolution with convection-allowing grid spacings in the WRF*. *Wea. Forecasting*, **28**, 994-1018, https://doi.org/10.1175/waf-d-13-00005.1.

Dudhia, J., 1989: Numerical study of convection observed during the winter monsoon experiment using a mesoscale two-dimensional model. *J. Atmos. Sci.*, **46**, 3077-3107, https://doi.org/10.1175/1520-0469(1989)046%3C3077:nsocod%3E2.0.co;2.

Fowle, M. A., and P. J. Roebber, 2003: Short-range (0-48h) numerical prediction of convective occurrence, mode, and location. *Wea. Forecasting*, **18**, 782-794, https://doi.org/10.1175/1520-0434(2003)018%3C0782:SHNPOC%3E2.0.CO;2.

Gallo, B. T., and Coauthors, 2017: Breaking new ground in severe weather prediction: The 2015 NOAA/Hazardous weather testbed spring forecasting experiment. *Wea. Forecasting*, **32**, 1541-1568, https://doi.org/10.1175/waf-d-16-0178.1.

Gallus, W. A., N. A. Snook, and E. V. Johnson, 2008: Spring and summer severe weather reports over the Midwest as a function of convective mode: A preliminary study. *Wea. Forecasting*, **23**, 101-113, https://doi.org/10.1175/2007waf2006120.1.

Geerts, B., and Coauthors, 2017: The 2015 plains elevated convection at night field project. *Bull. Amer. Meteor. Soc.*, **98**, 767-786, https://doi.org/10.1175/bams-d-15-00257.1.

Guyer, J. L., and I. L. Jirak, 2014: The utility of storm-scale ensemble forecasts of cool season severe weather events from the SPC perspective. *27th Conf. on Severe Local Storms*, Madison, WI, Amer. Meteor. Soc., 37, https://ams.confex.com/ams/27SLS/webprogram/Paper254640.html.

Hawblitzel, D. P., F. Zhang, Z. Meng, and C. A. Davis, 2007: Probabilistic evaluation of the dynamics and predictability of the mesoscale convective vortex of 10-13 June 2003. *Mon. Wea. Rev.*, **135**, 1544-1563, https://doi.org/10.1175/mwr3346.1.

Helmus, J. J., and S. M. Collis, 2016: The Python ARM radar toolkit (Py-ART), a library for working with radar data in the python programming language. *J. Open Software Res.*, **4**, https://doi.org/10.5334/jors.119.

Hitchcock, S. M., R. S. Schumacher, G. R. Herman, M. C. Coniglio, M. D. Parker, and C. L. Ziegler, 2019: Evolution of pre- and postconvective environmental profiles from mesoscale convective systems during PECAN. *Mon. Wea. Rev.*, **147**, 2329-2354, https://doi.org/10.1175/mwr-d-18-0231.1.

Hong, S.-Y., and J.-O. J. Lim, 2006: The WRF single-moment 6-class microphysics scheme (WSM6). *J. Korean Meteor. Soc.*, **42**, 129-151.

Hong, S.-Y., Y. Noh, and J. Dudhia, 2006: A new vertical diffusion package with an explicit treatment of entrainment processes. *Mon. Wea. Rev.*, **134**, 2318-2341, https://doi.org/10.1175/mwr3199.1.

James, R. P., J. M. Fritsch, and P. M. Markowski, 2005: Environmental distinctions between cellular and slabular convective lines. *Mon. Wea. Rev.*, **133**, 2669-2691, https://doi.org/10.1175/mwr3002.1.

Jiménez, P. D., J. Dudhia, J. F. González-Rouco, J. Navarro, J. P. Montávez, and E. García-Bustamante, 2012: A revised scheme for the WRF surface layer formulation. *Mon. Wea. Rev.*, **140**, 898-918, https://doi.org/10.1175/mwr-d-11-00056.1.

Jirak, I. L., and W. R. Cotton, 2007: Observational analysis of the predictability of mesoscale convective systems. *Wea. Forecasting*, **22**, 813-838, https://doi.org/10.1175/waf1012.1.

Kain, J. S., 2004: The Kain-Fritsch convective parameterization: An update. *J. Appl. Meteor.*, **43**, 170-181, https://doi.org/10.1175/1520-0450(2004)043%3C0170:tkcpau%3E2.0.co;2.

Mallinson, H. M., and S. G. Lasher-Trapp, 2019: An investigation of hydrometeor latent cooling upon convective cold pool formation, sustainment, and properties. *Mon. Wea. Rev.*, **147**, 3205-3222, https://doi.org/10.1175/mwr-d-18-0382.1.

Mansell, E. R., C. L. Ziegler, and E. C. Bruning, 2010: Simulated electrification of a small thunderstorm with two-moment bulk microphysics. *J. Atmos. Sci.*, **67**, 171-194, https://doi.org/10.1175/2009jas2965.1.

Marion, G. R., and R. J. Trapp, 2019: The dynamical coupling of convective updrafts, downdrafts, and cold pools in simulated supercell thunderstorms. *J. Geophys. Res. Atmos.*, **124**, 664-683, https://doi.org/10.1029/2018jd029055.

McAnelly, R. L., J. E. Nachamkin, W. R. Cotton, and M. E. Nicholls, 1997: Upscale evolution of MCSs: Doppler radar analysis and analytical investigation. *Mon. Wea. Rev.*, **125**, 1083-1110, https://doi.org/10.1175/1520-0493(1997)125%3C1083:ueomdr%3E2.0.co;2.

Mendenhall, W., and T. Sincich, 2007: *Statistics for Engineering and the Sciences*. 5th ed. Pearson-Prentice Hall, 1060 pp.

Mlawer, E. J., S. J. Taubman, P. D. Brown, M. J. Iacono, and S. A. Clough, 1997: Radiative transfer for inhomogeneous atmospheres: RRTM, a validated correlated-k model for the longwave. *J. Geophys. Res.*, **102**, 16663-16682, https://doi.org/10.1029/97jd00237.

Morrison, H., G. Thompson, and V. Tatarskii, 2009: Impact of cloud microphysics on the development of trailing stratiform in a simulated squall line: Comparison of one- and two-moment schemes. *Mon. Wea. Rev.*, **137**, 991-1007, https://doi.org/10.1175/2008mwr2556.1.

Mulholland, J. P., S. W. Nesbitt, and R. J. Trapp, 2019: A case study of terrain influences on upscale convective growth of a supercell. *Mon. Wea. Rev.*, **147**, 4305-4324, https://doi.org/10.1175/mwr-d-19-0099.1.

Nielsen, E. R., G. R. Herman, R. C. Tournay, J. M. Peters, and R. S. Schumacher, 2015: Double impact: When both tornadoes and flash floods threaten the same place at the same time. *Wea. Forecasting*, **30**, 1673-1693, https://doi.org/10.1175/waf-d-15-0084.1.

NOAA/NCEI, 2019: NCEP numerical weather prediction models Global Forecast System (GFS) grid 004. Subset used: May – June 2016, accessed 1 August 2019. [Available online at https://nomads.ncdc.noaa.gov/data/gfsanl/].

Parker, M. D., 2018: External vs. self-organization of nocturnal MCSs from PECAN. *29th Conf. on Severe Local Storms*, Stowe, VT, Amer. Meteor. Soc., 4.5, https://ams.confex.com/ams/29SLS/meetingapp.cgi/Paper/348312.

Parker, M. D., B. S. Borchardt, R. L. Miller, and C. L. Ziegler, 2020: Simulated evolution and severe wind production by the 25-26 June 2015 nocturnal MCS from PECAN. *Mon. Wea. Rev.*, **148**, 183-209, https://doi.org/10.1175/mwr-d-19-0072.1.

Peters, J. M., and R. S. Schumacher, 2015: The simulated structure and evolution of a quasi-idealized warm-season convective system with a training convective line. *J. Atmos. Sci.*, **72**, 1987-2010, https://doi.org/10.1175/jas-d-14-0215.1.

Peters, J. M., and R. S. Schumacher, 2016: Dynamics governing a simulated mesoscale convective system with a training convective line. J. Atmos. Sci., 73, 2643-2664, https://doi.org/10.1175/jas-d-15-0199.1.

Peters, J. M., K. C. Eure, and R. S. Schumacher, 2017: Factors that drive MCS growth from supercells. *17th Conf. on Mesoscale Processes*, San Diego, CA, Amer. Meteor. Soc., 9.6, https://ams.confex.com/ams/17MESO/webprogram/Paper320248.html.

Rotunno, R., J. B. Klemp, and M. L. Weisman, 1988: A theory for strong, long-lived squall lines. *J. Atmos. Sci.*, **45**, 463-485, https://doi.org/10.1175/1520-0469(1988)045%3C0463:atfsll%3E2.0.co;2.

Schumacher, R. S., 2015: Resolution dependence of initiation and upscale growth of deep convection in convection-allowing forecasts of the 31 May-1 June 2013 supercell and MCS. *Mon. Wea. Rev.*, **143**, 4331-4354, https://doi.org/10.1175/mwr-d-15-0179.1.

Schwartz, C. S., and Coauthors, 2009: Next-day convection-allowing WRF model guidance: A second look at 2-km versus 4-km grid spacing. *Mon. Wea. Rev.*, **137**, 3351-3372, https://doi.org/10.1175/2009mwr2924.1.

Skamarock, W. C., and Coauthors, 2019: A description of the advanced research WRF version 4. *NCAR Tech. Note NCAR/TN-556+STR*, 145pp. https://doi.org/10.5065/1dfh-6p97.

Smith, B. T., R. L. Thompson, J. S. Grams, C. Broyles, and H. E. Brooks, 2012: Convective modes for significant severe thunderstorms in the contiguous United States. Part I: Storm classification and climatology. *Wea. Forecasting*, **27**, 1114-1135, https://doi.org/10.1175/waf-d-11-00115.1.

Squitieri, B. J., and W. A. Gallus, 2016: WRF forecasts of Great Plains nocturnal low-level jet-driven MCSs. Part I: Correlation between low-level jet forecast accuracy and MCS precipitation forecast skill. *Wea. Forecasting*, **31**, 1301-1323, https://doi.org/10.1175/waf-d-15-0151.1.

Squitieri, B. J., and W. A. Gallus, 2020: On the forecast sensitivity of MCS cold pools and related features to horizontal grid spacing in convection-allowing WRF simulations. *Wea. Forecasting*, **35**, 325-346, https://doi.org/10.1175/waf-d-19-0016.1.

Tewari, M. F., and Coauthors, 2004: Implementation and verification of the unified NOAH land surface model in the WRF model. *20th Conf. on Weather Analysis and Forecasting/16th Conf. on Numerical Weather Prediction*, Seattle, WA, Amer. Meteor. Soc., 14.2a, https://ams.confex.com/ams/84Annual/webprogram/Paper69061.html.

Thielen, J. E., and W. A. Gallus, 2019: Influences of horizontal grid spacing and microphysics on WRF forecasts of convective morphology evolution for nocturnal MCSs in weakly forced environments. *Wea. Forecasting*, **34**, 1495-1517, https://doi.org/10.1175/waf-d-18-0210.1.

Thompson, G., P. R. Field, R. M. Rasmussen, and W. D. Hall, 2008: Explicit forecasts of winter precipitation using an improved bulk microphysics scheme. Part II: Implementation of a new snow parameterization. *Mon. Wea. Rev.*, **136**, 5095-5115, https://doi.org/10.1175/2008mwr2387.1.

Thompson, R. L., R. Edwards, J. A. Hart, K. L. Elmore, and P. Markowski, 2003: Close proximity soundings within supercell environments obtained from the Rapid Update Cycle. *Wea. Forecasting*, **18**, 1243-1261, https://doi.org/10.1175/1520-0434(2003)018%3C1243:cpswse%3E2.0.co;2.

Thompson, R. L., B. T. Smith, J. S. Grams, A. R. Dean, and C. Broyles, 2012: Convective modes for significant severe thunderstorms in the contiguous United States. Part II: Supercell and QLCS tornado environments, https://doi.org/10.1175/WAF-D-11-00116.1.

Weisman, M. L., 1992: The role of convectively generated rear-inflow jets in the evolution of long-lived mesoconvective systems. *J. Atmos. Sci*., **49**, 1826-1847, https://doi.org/10.1175/1520-0469(1992)049%3C1826:trocgr%3E2.0.co;2.

Weisman, M. L., W. C. Skamarock, and J. B. Klemp, 1997: The resolution dependence of explicitly modeled convective systems. *Mon. Wea. Rev*., **125**, 527-548 https://doi.org/10.1175/1520-0493(1997)125%3C0527:trdoem%3E2.0.co;2.

Weisman, M. L., and R. Rotunno, 2004: "A theory for strong long-lived squall lines" revisited. *J. Atmos. Sci.*, **61**, 361-382, https://doi.org/10.1175/1520-0469(2004)061%3C0361:atfsls%3E2.0.co;2.

Weisman, M. L., C. Davis, W. Wang, K. W. Manning, and J. B. Klemp, 2008: Experiences with 0-36-h explicit convective forecasts with the WRF-ARW model. *Wea. Forecasting*, **23**, 407-437, https://doi.org/10.1175/2007WAF2007005.1.

Weiss, S. J., M. E. Pyle, Z. Janjic, D. R. Bright, and G. J. DiMego, 2008: The operational high resolution window WRF model runs at NCEP: Advantages of multiple model runs for severe convective weather forecasting. *24th Conf. on Severe Local Storms*, Savannah, GA, Amer. Meteor. Soc., P10.8, https://ams.confex.com/ams/pdfpapers/142192.pdf.

3.8 Tables

Table 1: All UCG and non-UCG cases used, along with the specific model focus area.

Date	Event Type	Focus Area
05-16	UCG	OK
05-21	non-UCG	W KS
05-29	non-UCG	NW TX
05-30	UCG	KS/NE
05-31	non-UCG	OK
06-04	non-UCG	OK
06-06	non-UCG	KS/NE
06-08	non-UCG	CO/KS/NE
06-12	UCG	CO/KS/NE
06-13	UCG	OK
06-17	UCG	KS/NE
06-18	non-UCG	KS
06-21	UCG	SD
06-25	UCG	KS
06-27	non-UCG	CO/KS/NE
06-28	UCG	CO/KS/NE
06-29	non-UCG	IA
07-01	UCG	CO/KS
07-05	UCG	KS/NE
07-06	UCG	NE/SD
07-07	non-UCG	CO/KS/NE
07-09	non-UCG	NE/SD
07-11	UCG	NE/IA
07-12	UCG	KS
07-29	non-UCG	CO/KS/NE
08-05	UCG	KS
08-06	UCG	CO/KS
08-08	non-UCG	NE/SD
08-09	non-UCG	OK
08-10	non-UCG	IA

Table 2: WRF-ARW setup used for all 30 cases.

Parameter	Outer Nests	Inner Nests	Notes/Reference
Horizontal Grid Spacing	27km/9km	3km	Inner Grid 1500x1500km, two-way feedback enabled
Vertical Sigma Levels	50	50	Squitieri and Gallus (2016)
Model top pressure	50 hPa	50 hPa	
IC/LBCs	GFS (0.5°)	GFS (0.5°)	
Cumulus Physics	Kain-Fritsch	None	Kain (2004)
Microphysics	Morrison	Morrison	Morrison et al. (2009)
Radiation	RRTM | Dudhia	RRTM | Dudhia	Mlawer et al. (1997) | Dudhia (1989)
PBL Physics	YSU	YSU	Hong et al. (2006)
Surface Layer Physics	MM5	MM5	Jiménez et al. (2012)
Land Surface	NOAH	NOAH	Tewari et al. (2004)
Simulation Time	24h	24h	12:00 UTC - 12:00 UTC

Table 3: CM1 Simulation setup

Parameter	**CM1 Simulation**
Horizontal Grid Spacing	0.25 km (200x150 km)
Vertical Levels	98
Vertical Grid Spacing	100-250m, stretched from 3-10km
Model Top	17km
Microphysics	Morrison
Turbulence	TKE-based subgrid closure
Land-surface	Free-slip bottom boundary
Initialization	Homogenous (based on input sounding), vertical line of 4 warm bubbles
Lateral Boundary	Open radiative
Simulation Time	6h
Other	Coriolis omitted

3.9 Figures

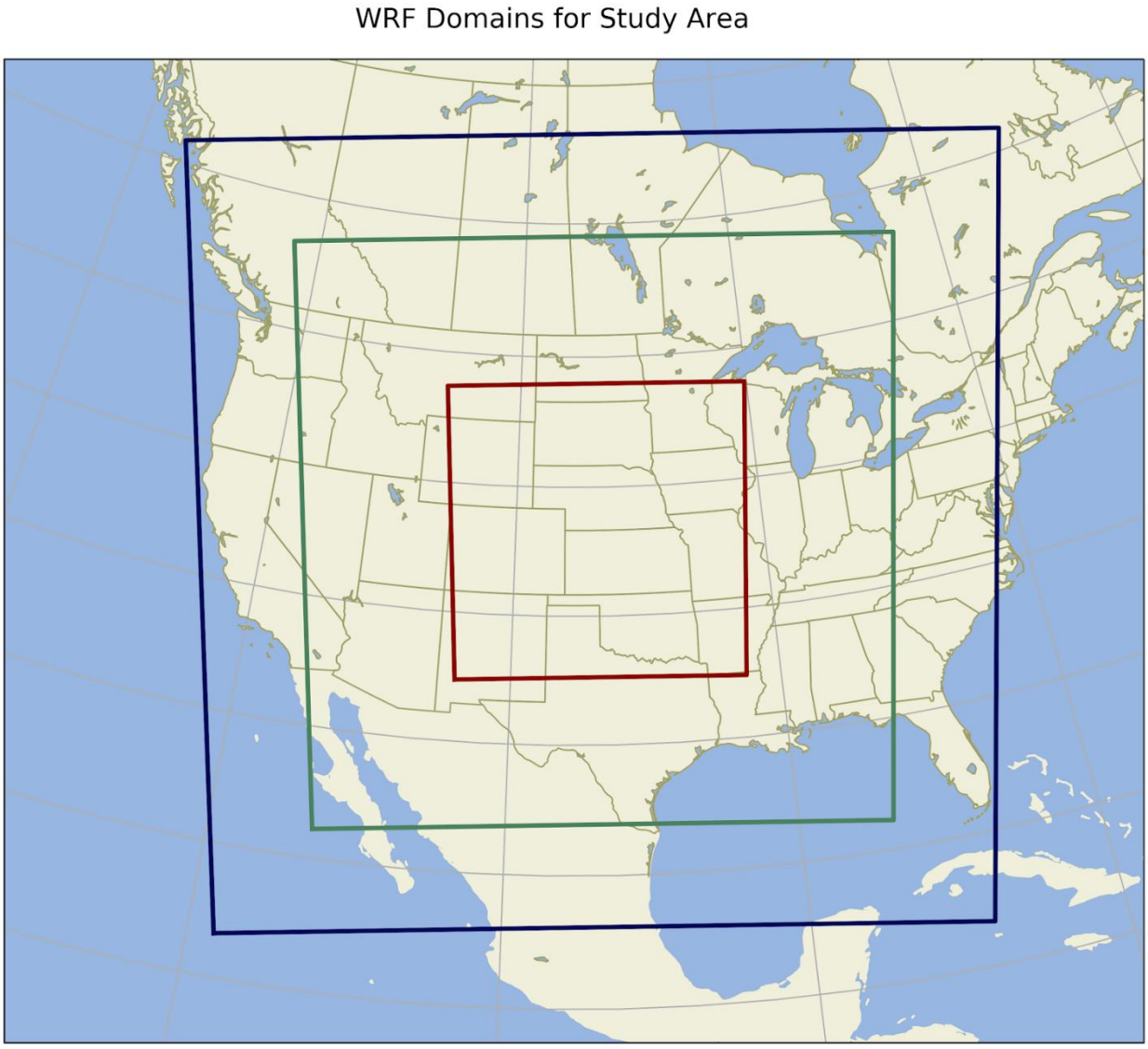

Figure 1: WRF domains used in this study. The 27km outer domain is denoted by dark blue, with inner 9km (3km) domains outlined in green (dark red), respectively.

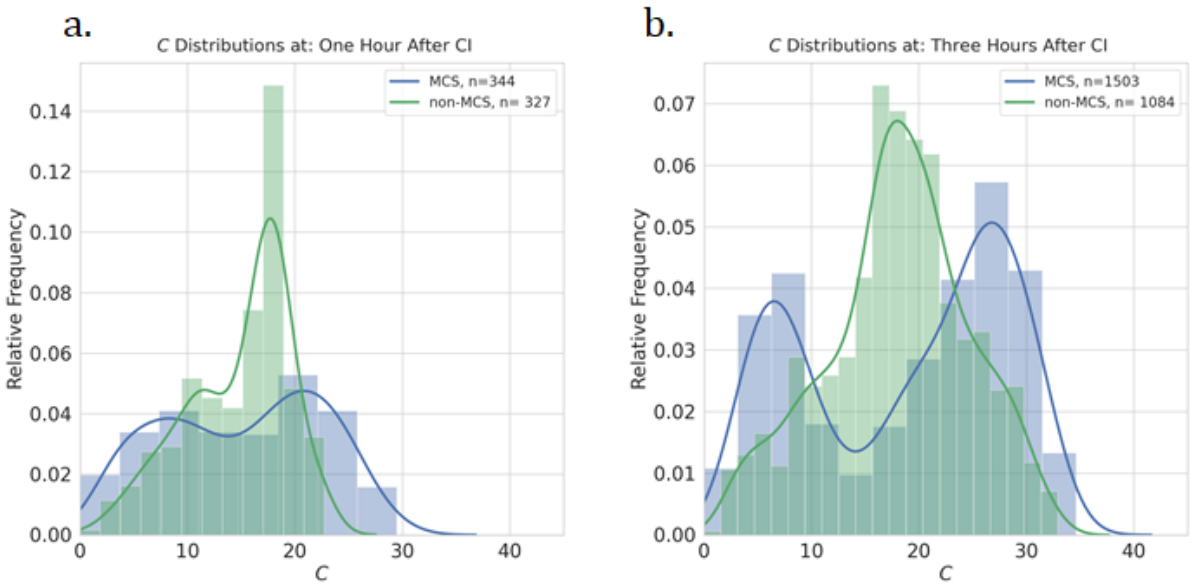

Figure 2: Histogram and kernel density estimate of the cold pool parameter C for UCG (blue) and non-UCG (green) sets of cases (a) one hour and (b) three hours after convective initiation for all cold pool grid points.

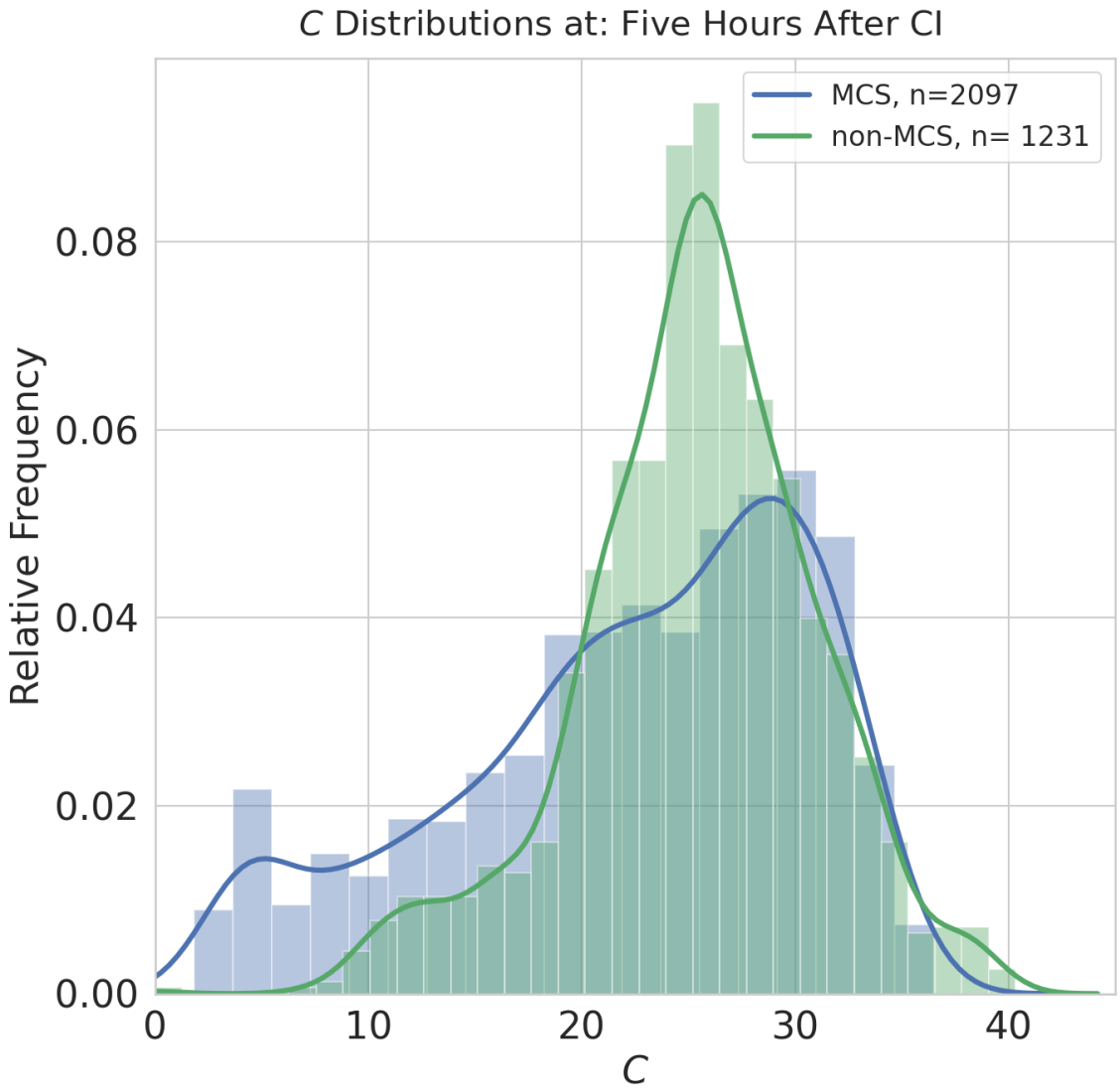

Figure 3: As in Fig. 2, but for five hours after convective initiation.

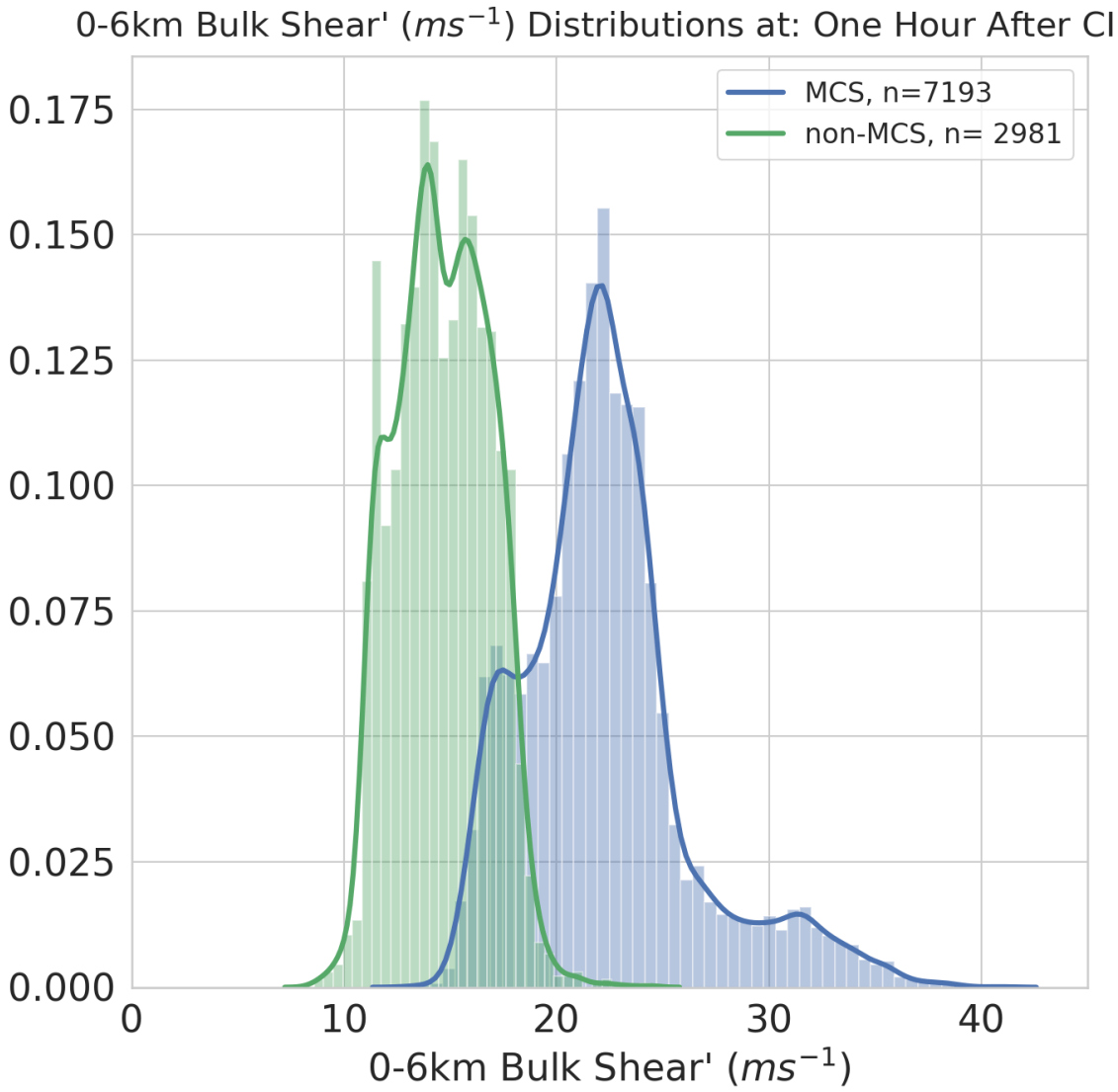

Figure 4: As in Fig. 2, but for 0-6km shear one hour after convective initiation.

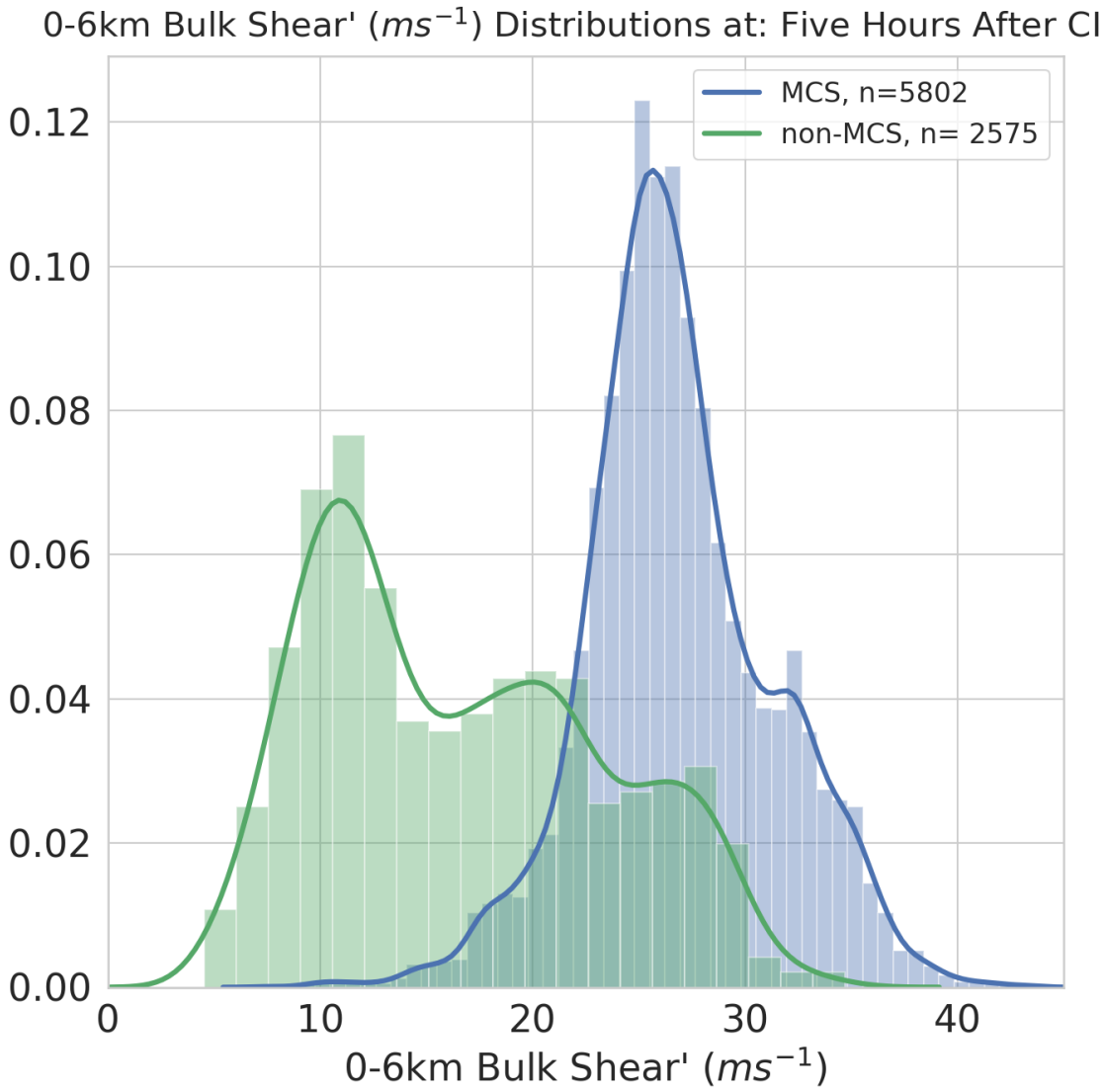

Figure 5: As in Fig. 4, but for five hours after convective initiation.

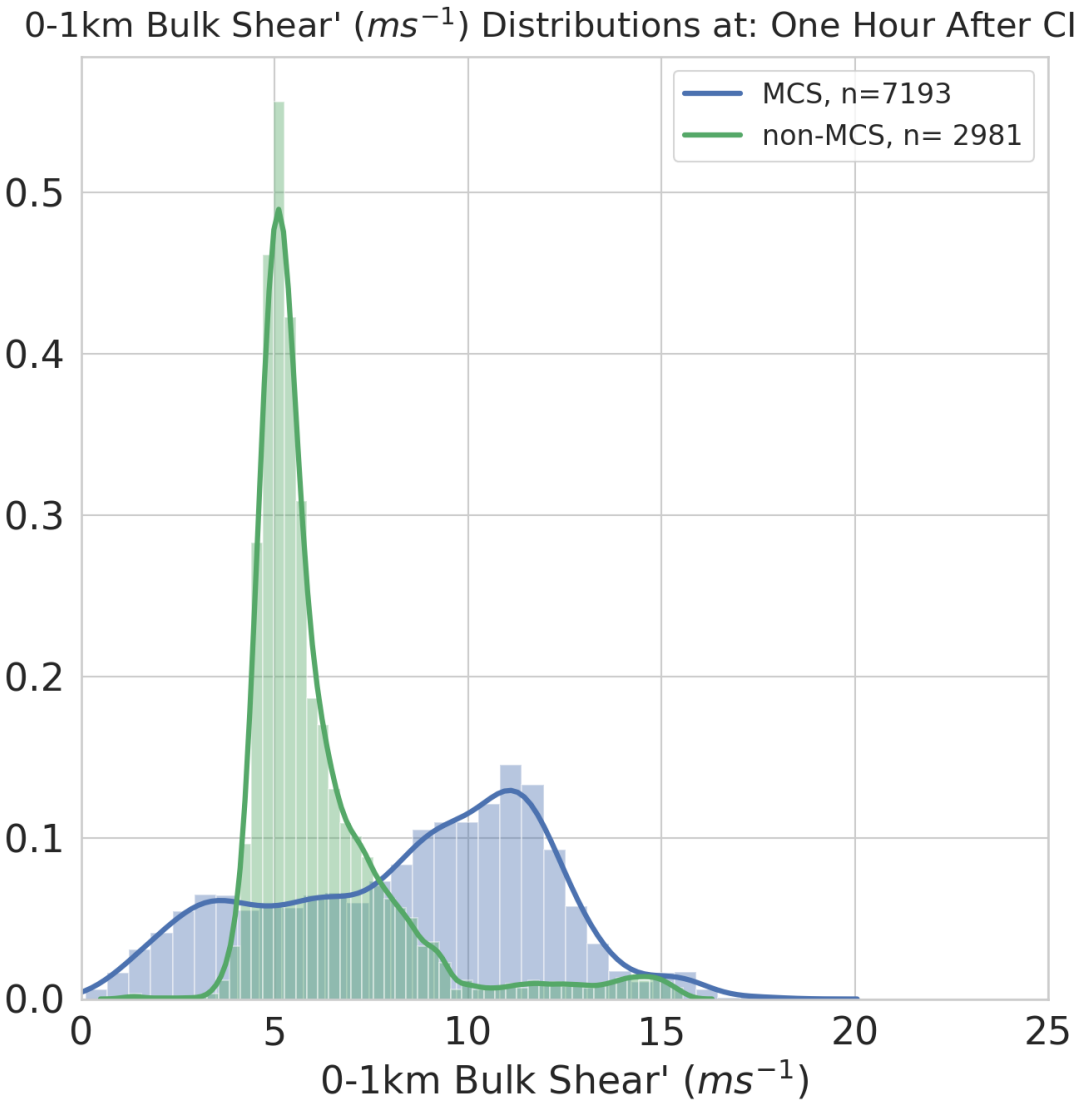

Figure 6: As in Fig. 4, except for 0-1km shear magnitudes.

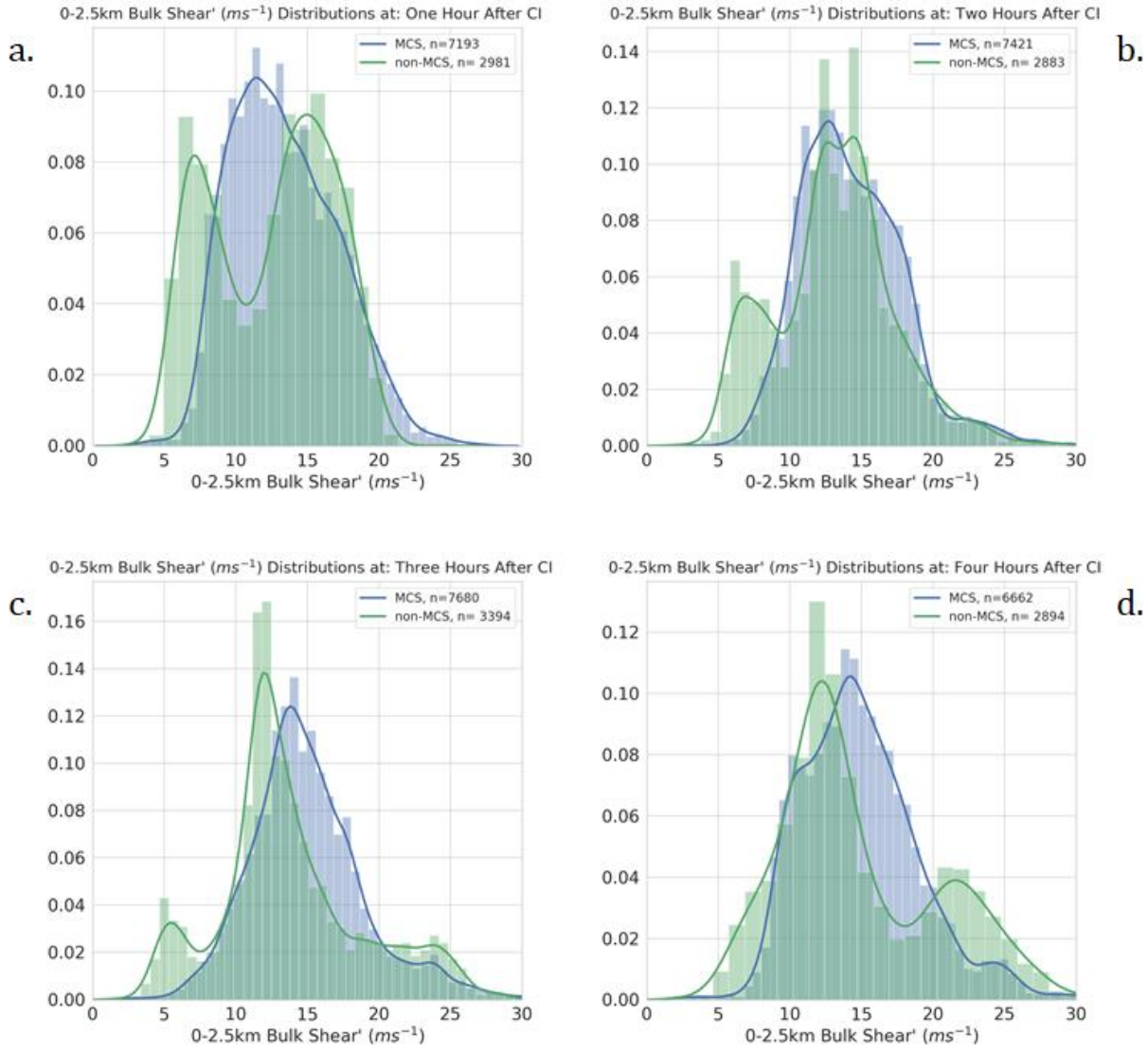

Figure 7: Histogram and kernel density estimates of 0-2.5km shear at (a) one hour, (b) two hours, (c) three hours, and (d) four hours after convective initiation for UCG events (blue) and non-UCG events (green).

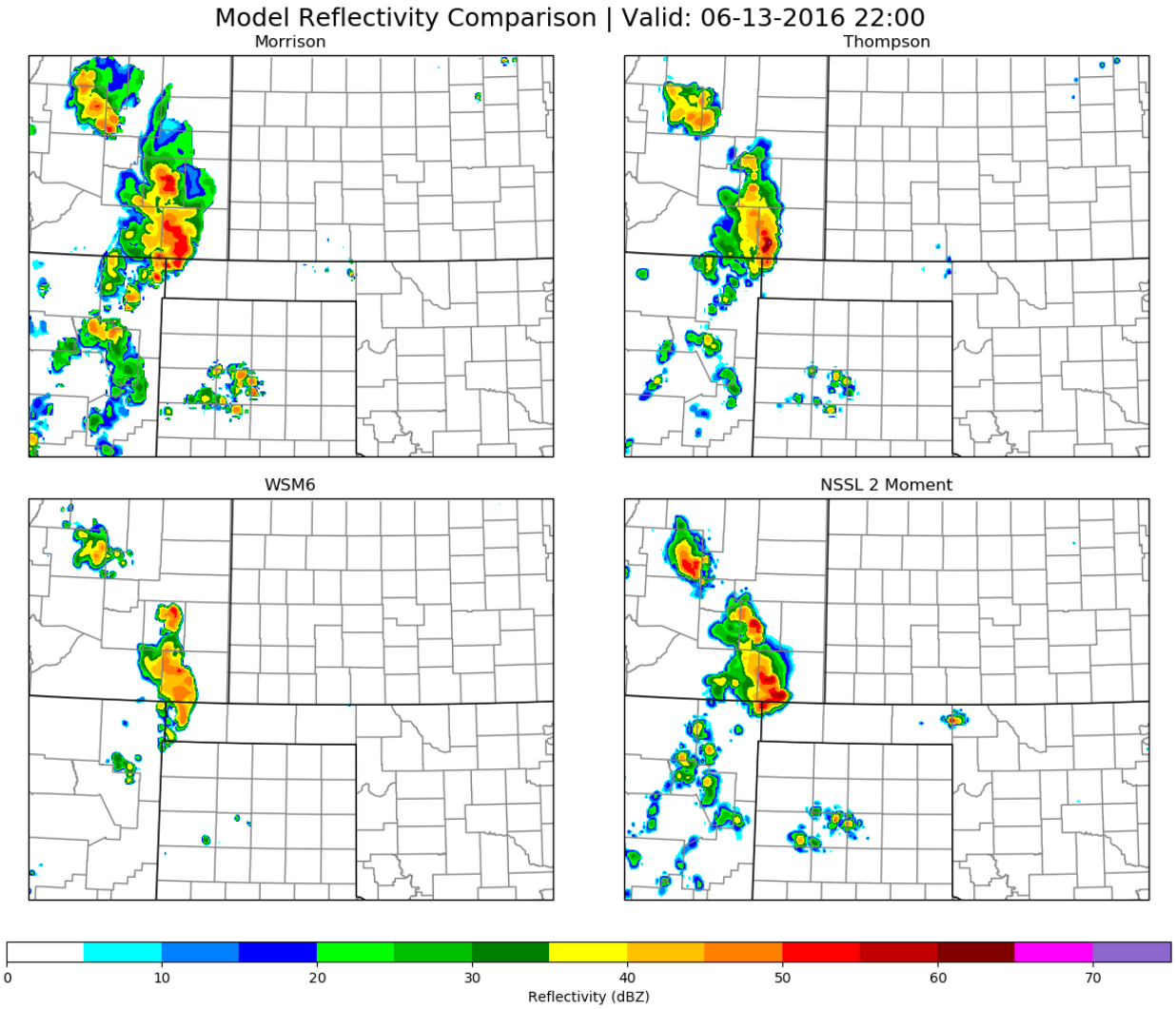

Figure 8: WRF simulated lowest model level reflectivity for a UCG event occurring 13 June 2016 five hours after convective initiation.

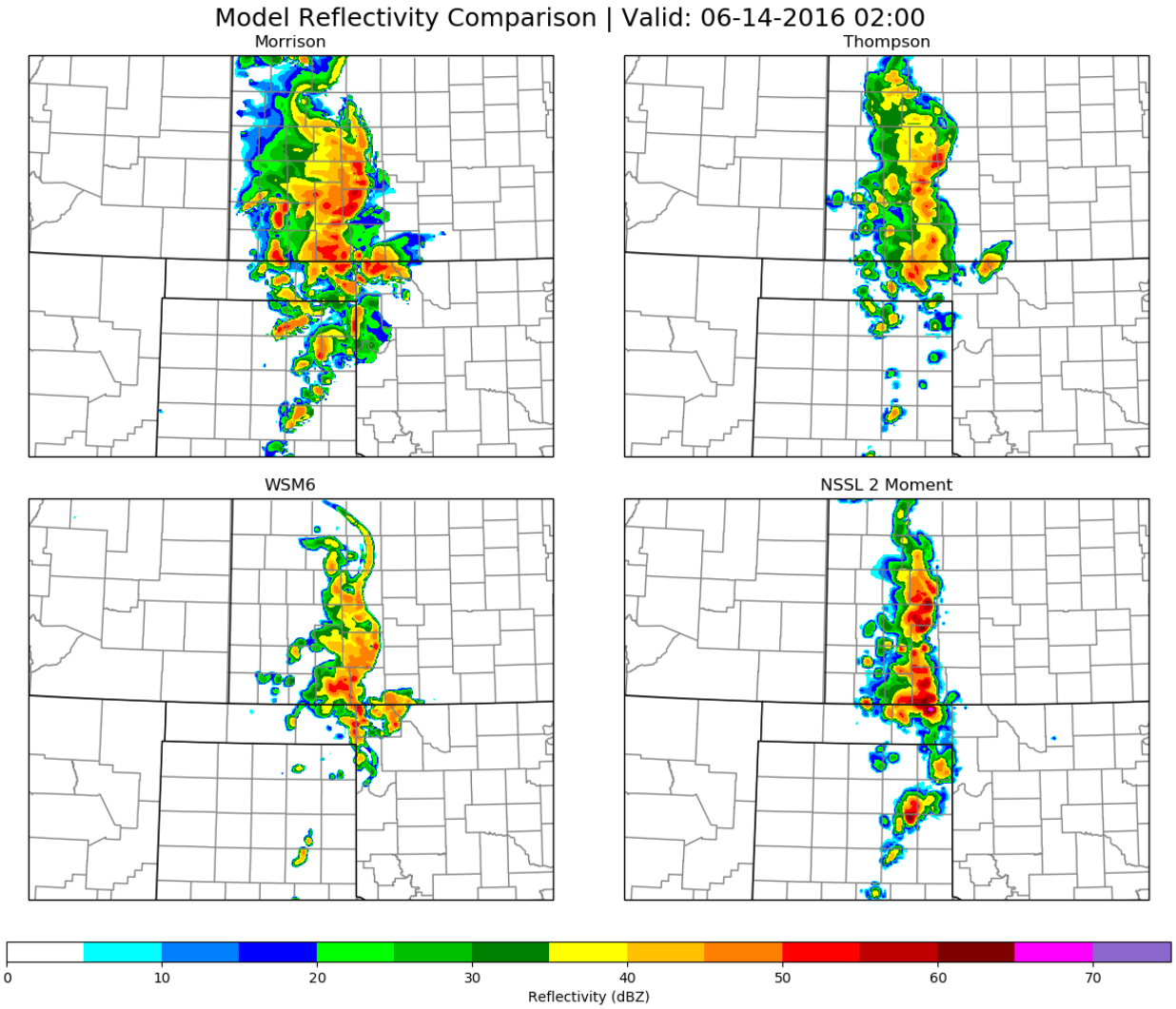

Figure 9: Same as Fig. 8, but for nine hours after convective initiation.

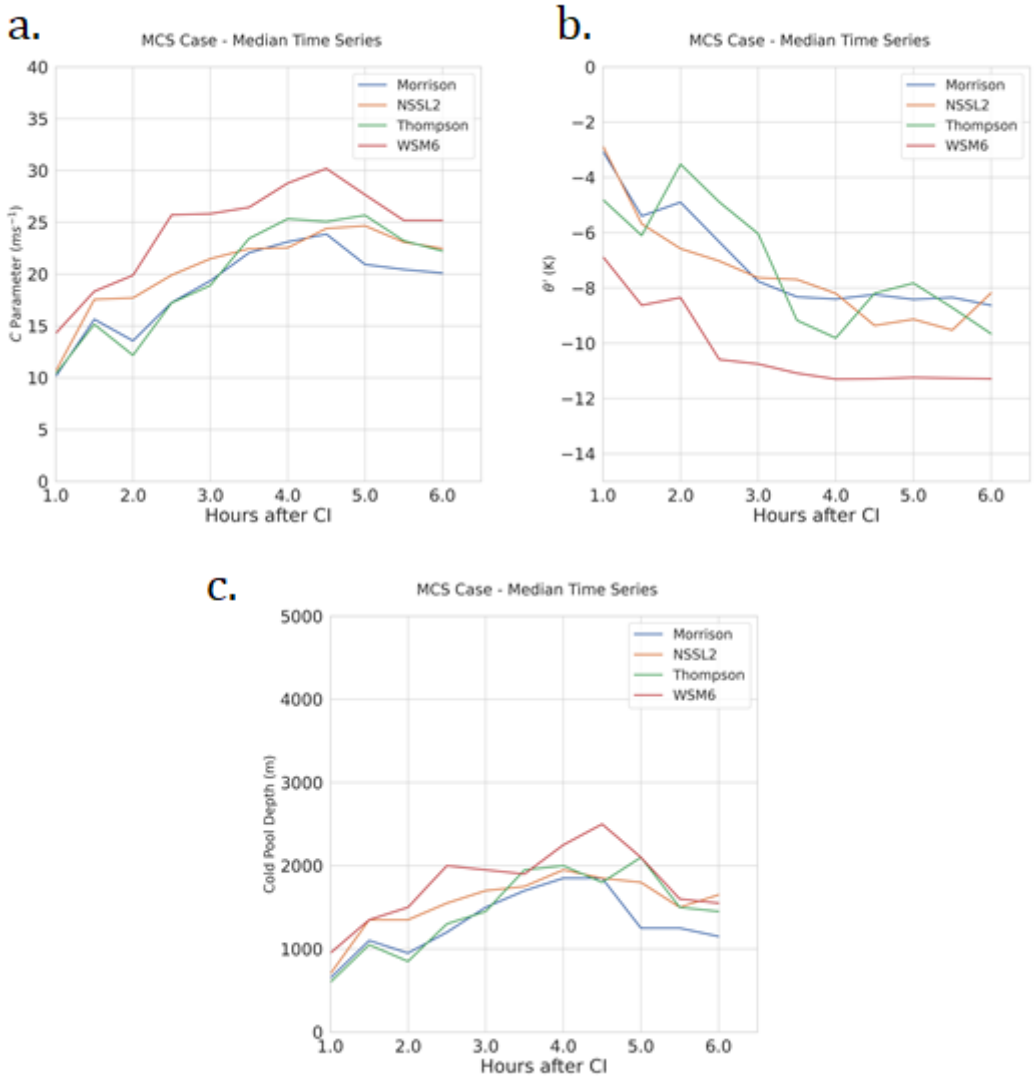

Figure 10: Median values of (a) cold pool parameter C, and (b) perturbation potential temperature (θ') over time for the UCG case of 13 June 2016 simulated in the WRF.

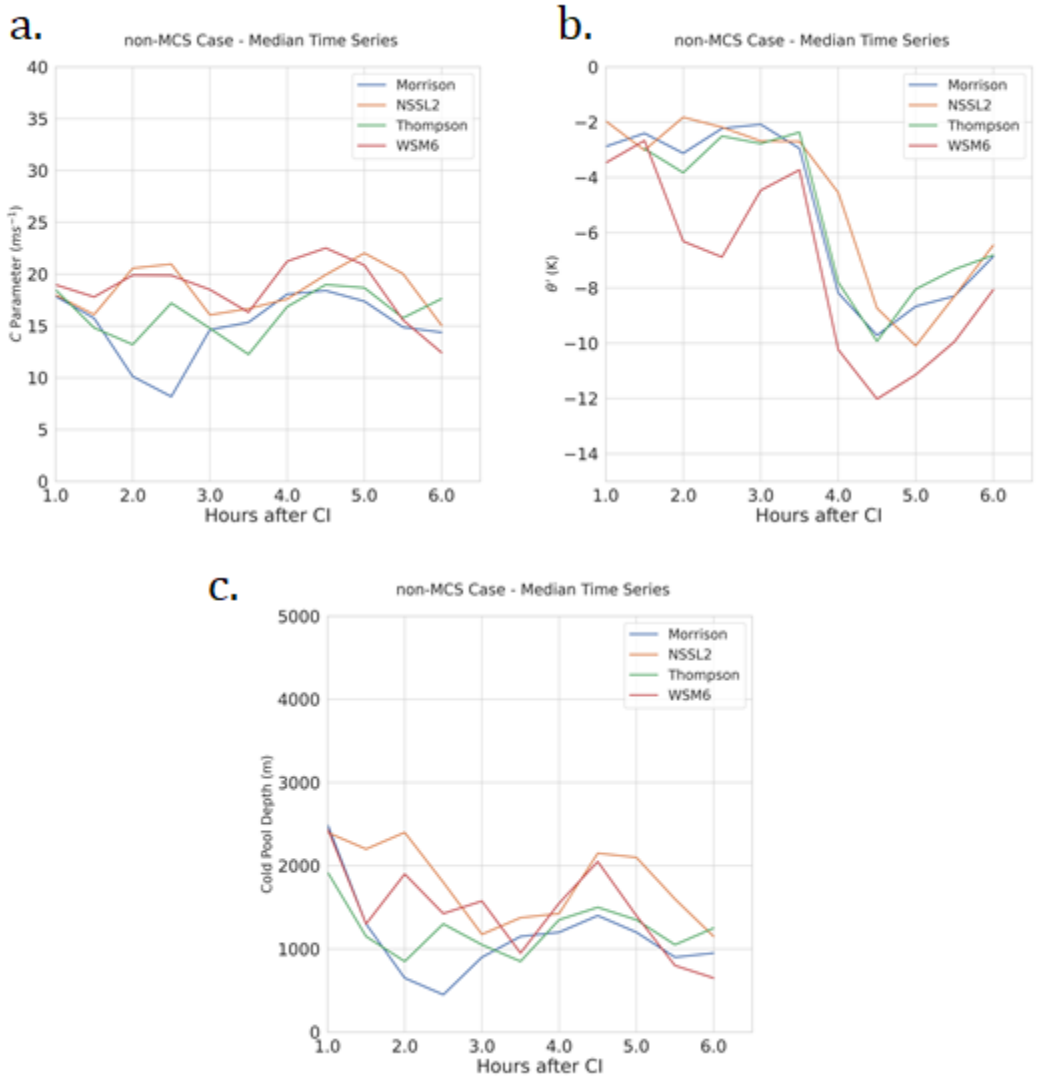

Figure 11: As in Fig. 10, but for the non-UCG event.

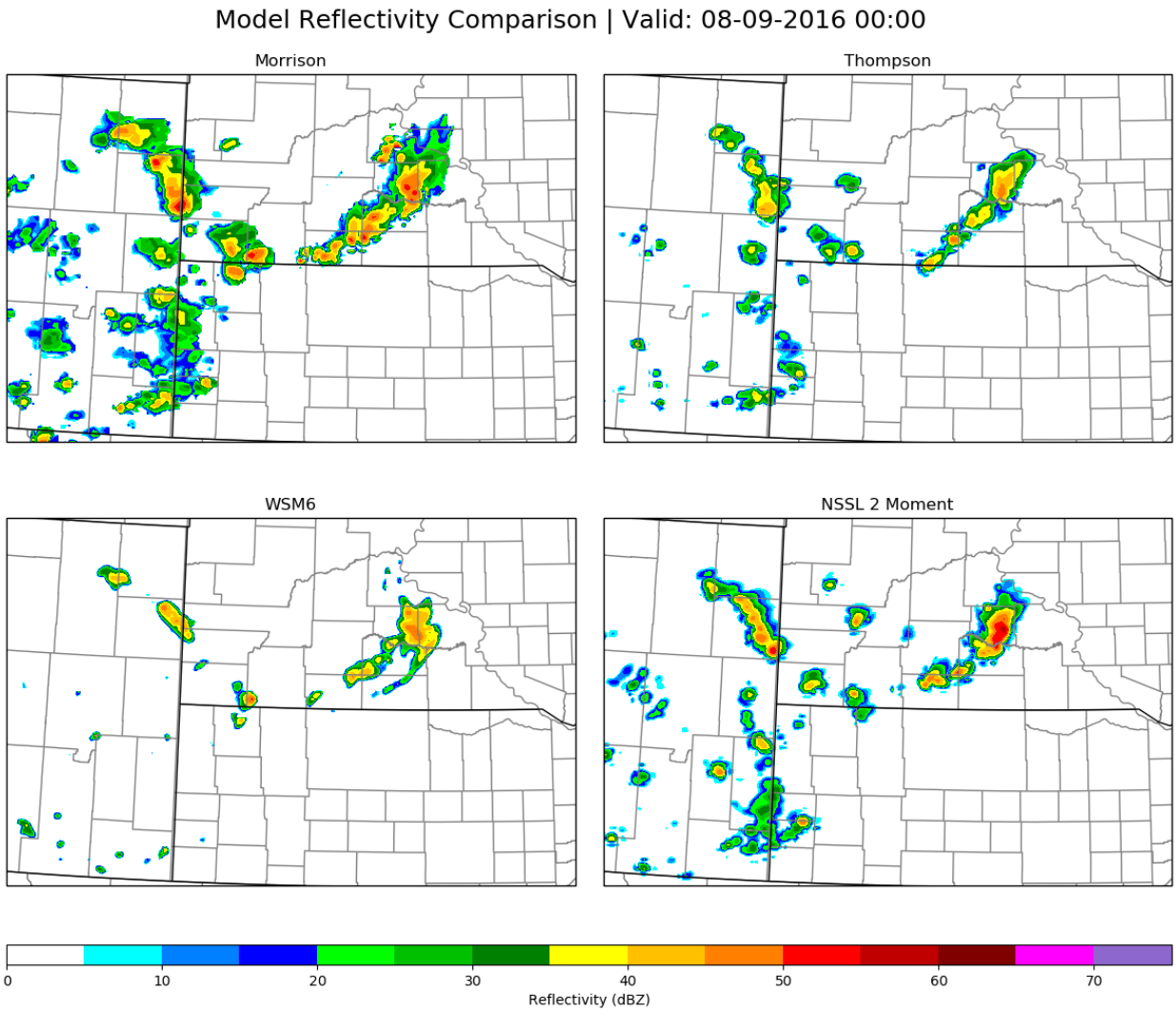

Figure 12: As in Fig. 8, but for a non-UCG event on 9 August 2016 four hours after convective initiation.

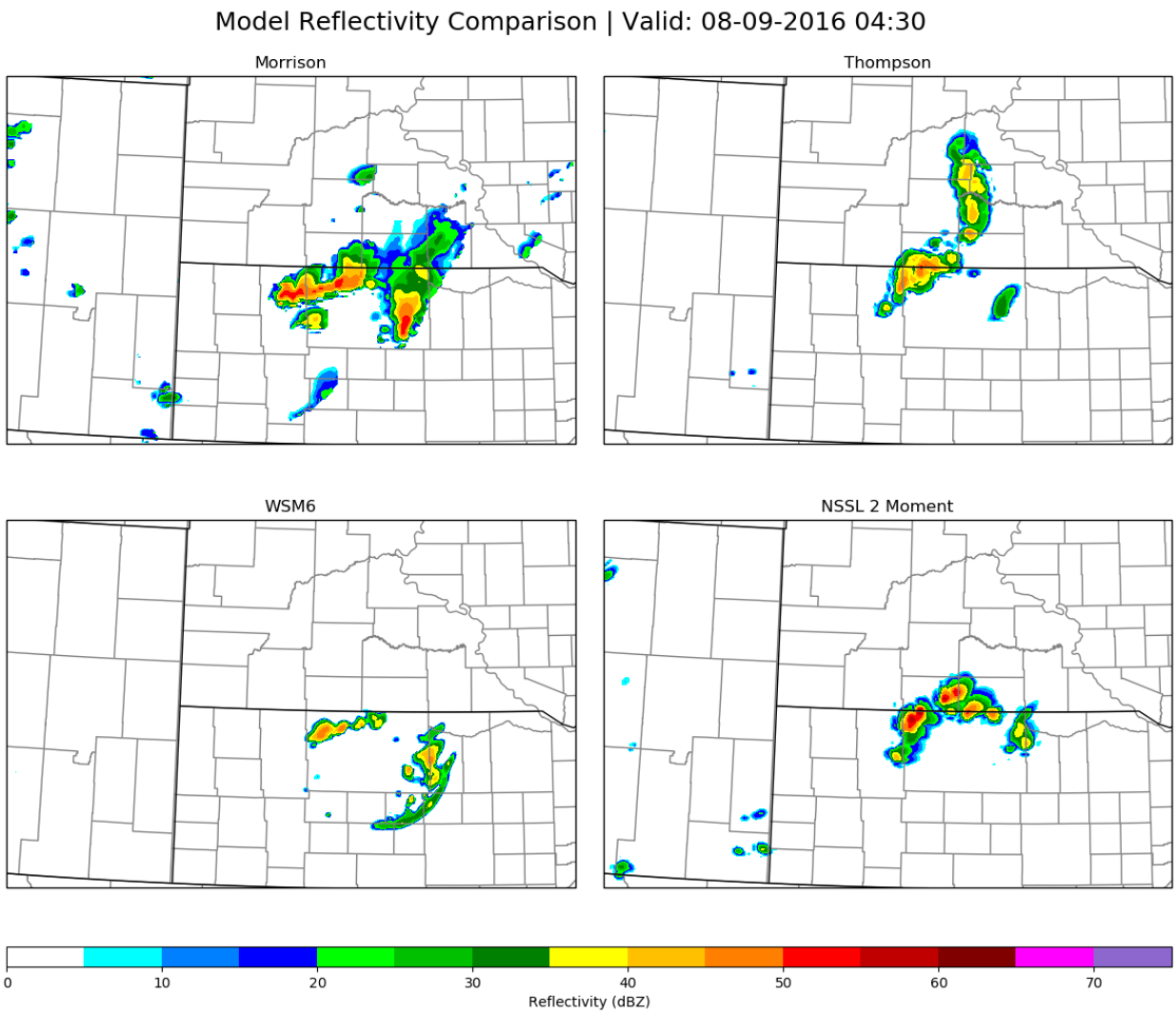

Figure 13: As in Fig. 12, but 8.5 hours after convective initiation.

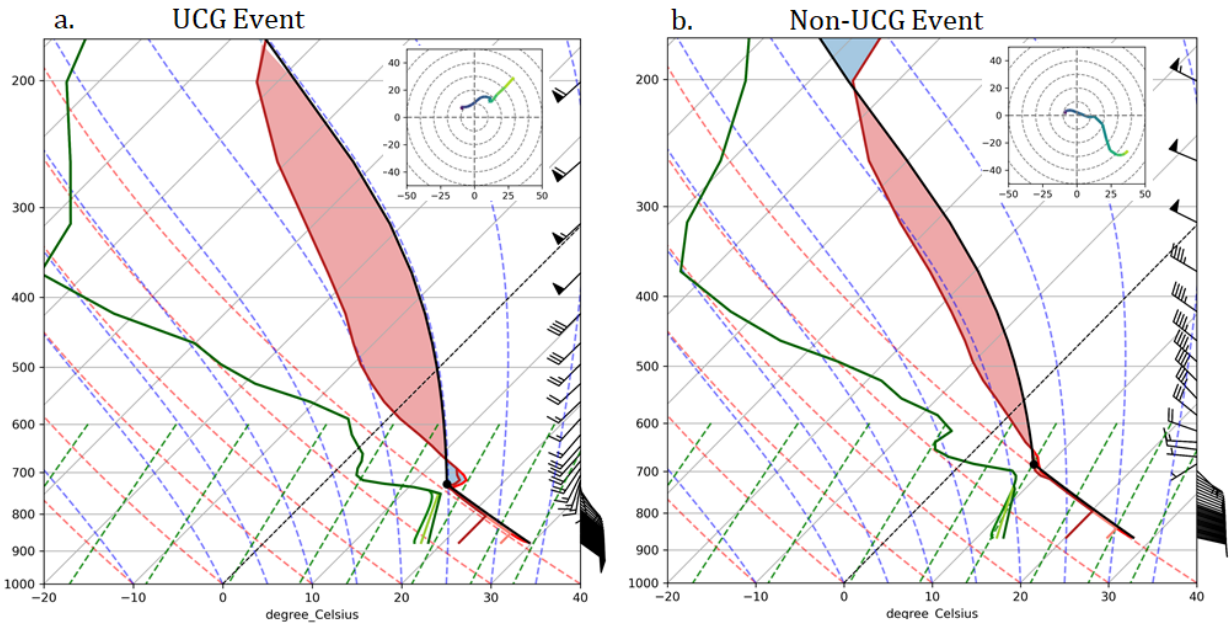

Figure 14: Skew-T/logP diagrams of baseline soundings used for initialization in the CM1 CTRL experiments in (a) the UCG event and (b) the non-UCG event. For both, the CTRL temperature (dewpoint) is represented by the red (green) line, and CAPE (CIN) is shaded in light red (light blue). Wind barbs on the right side of each skew-T are given in knots. In each hodograph, winds are plotted in knots from the surface to roughly 6km. The SBL250 experiment T (Td) is given by the light red (yellow-green) lines, and in SBL750 is represented by dark red (dark green).

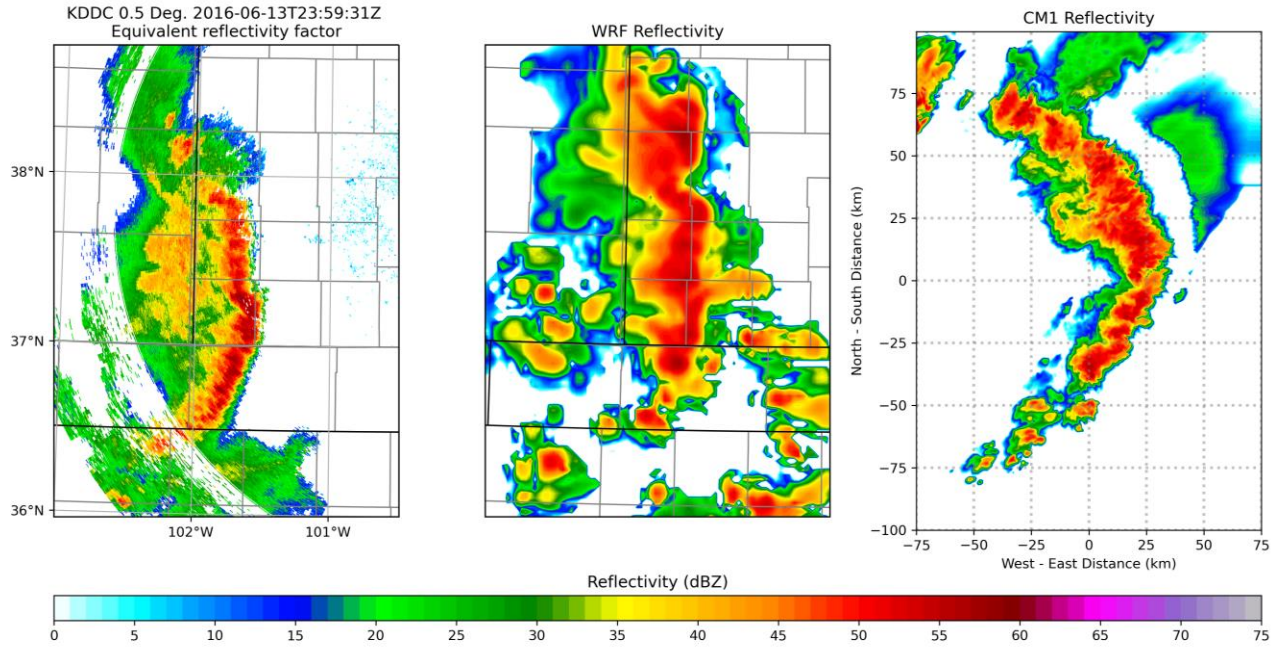

Figure 15: (a) Observed base reflectivity, and simulated lowest model-level reflectivity from (b) the WRF, and (c) the CTRL CM1 experiment for the UCG event. Observational radar data from the NCEI NEXRAD Inventory, plotted through Py-ART (Helmus and Collis, 2016).

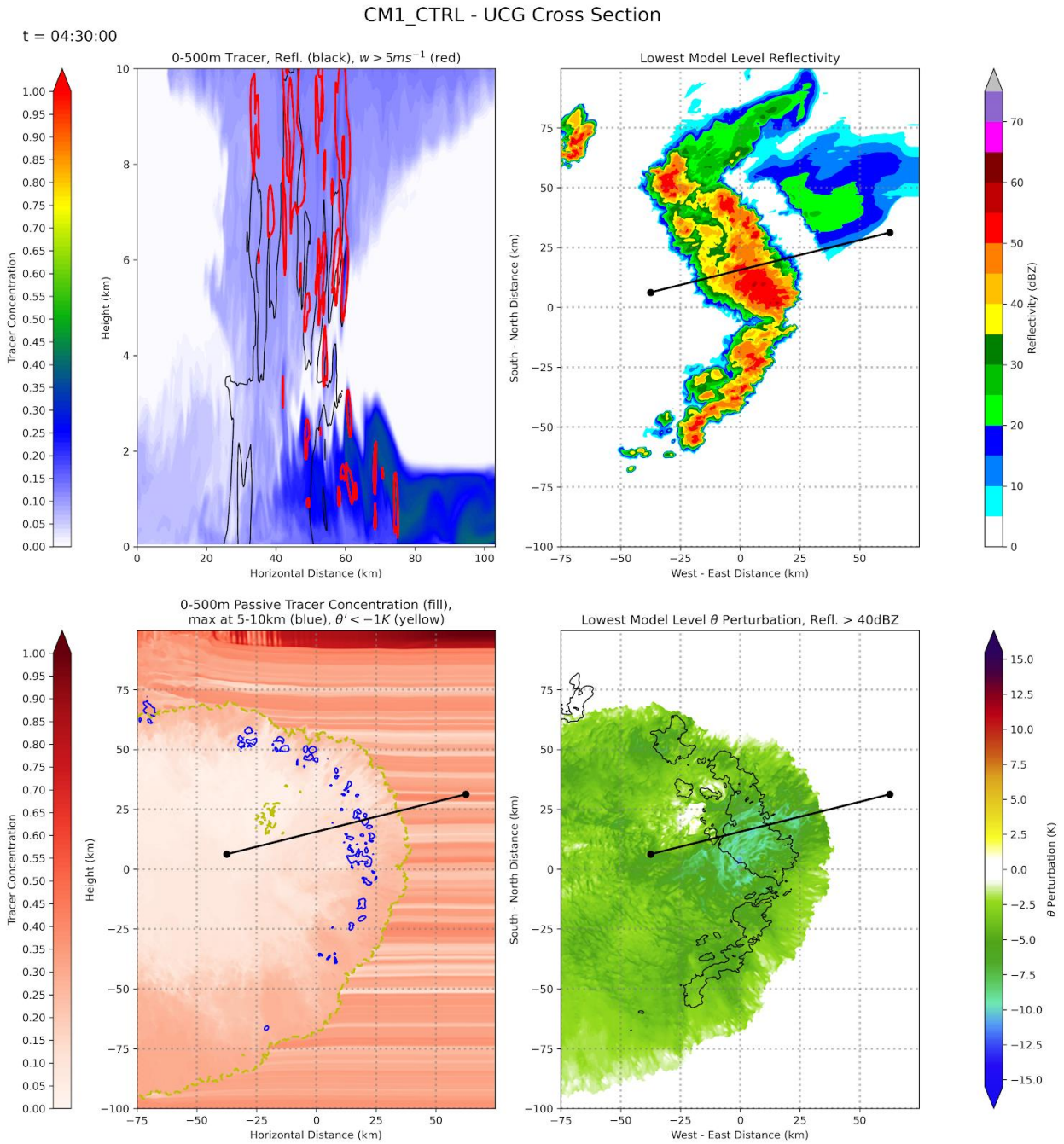

Figure 16: CM1 CTRL experiment results for the upscale growth event with (a) Cross-section of 0-500m tracer concentration, reflectivity, and vertical velocity, (b) Lowest model reflectivity, (c) 0-500m tracer concentration at the model surface, cold pool boundary, and surface tracer >0.20 in the 5-10km layer, and (d) surface potential temperature perturbation and reflectivity > 40dBZ (black outline), valid at t = 4.5hr. The cross section path is denoted by the black line in (b-d).

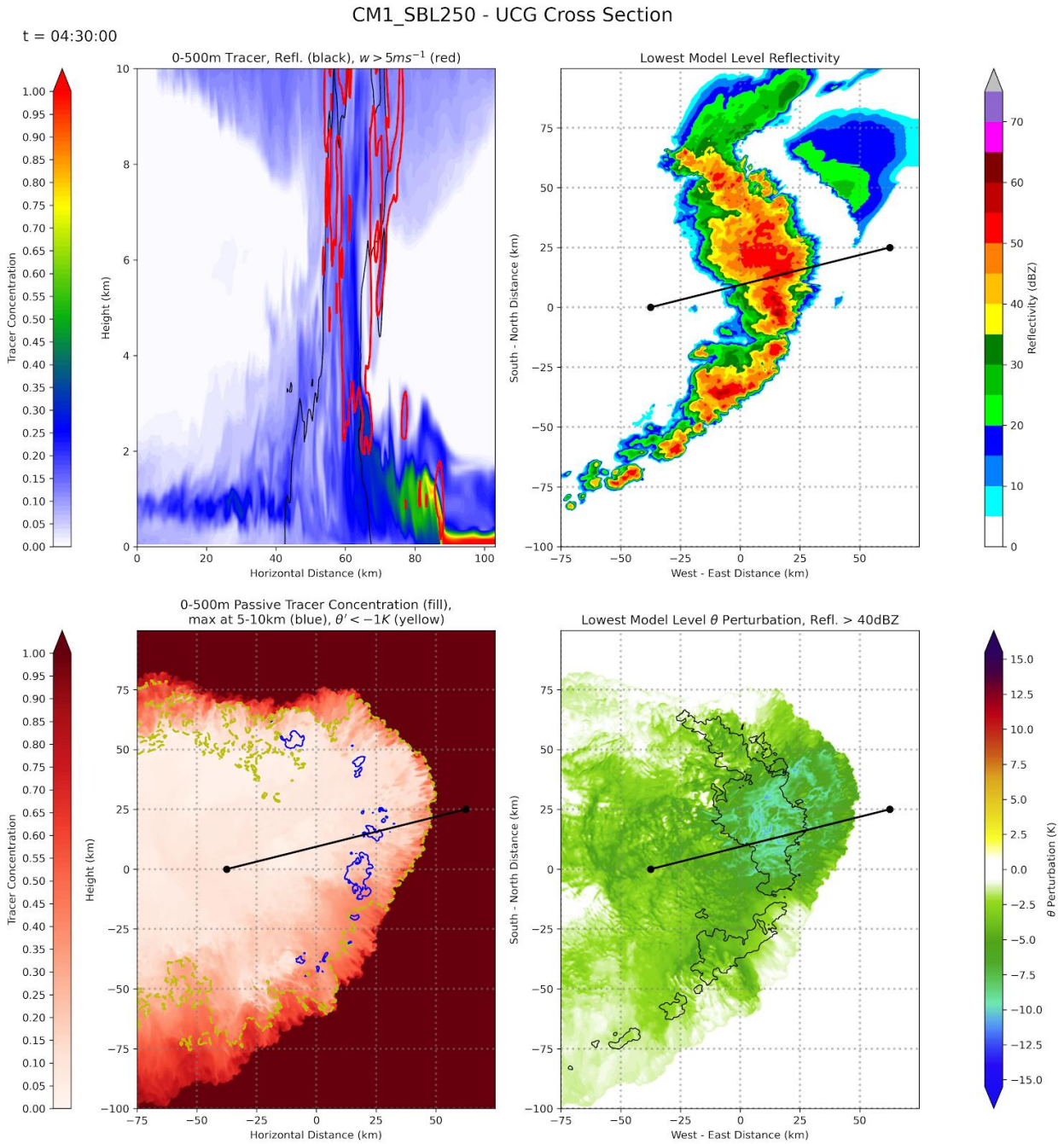

Figure 17: As in Fig. 16, but for the SBL250, UCG experiment.

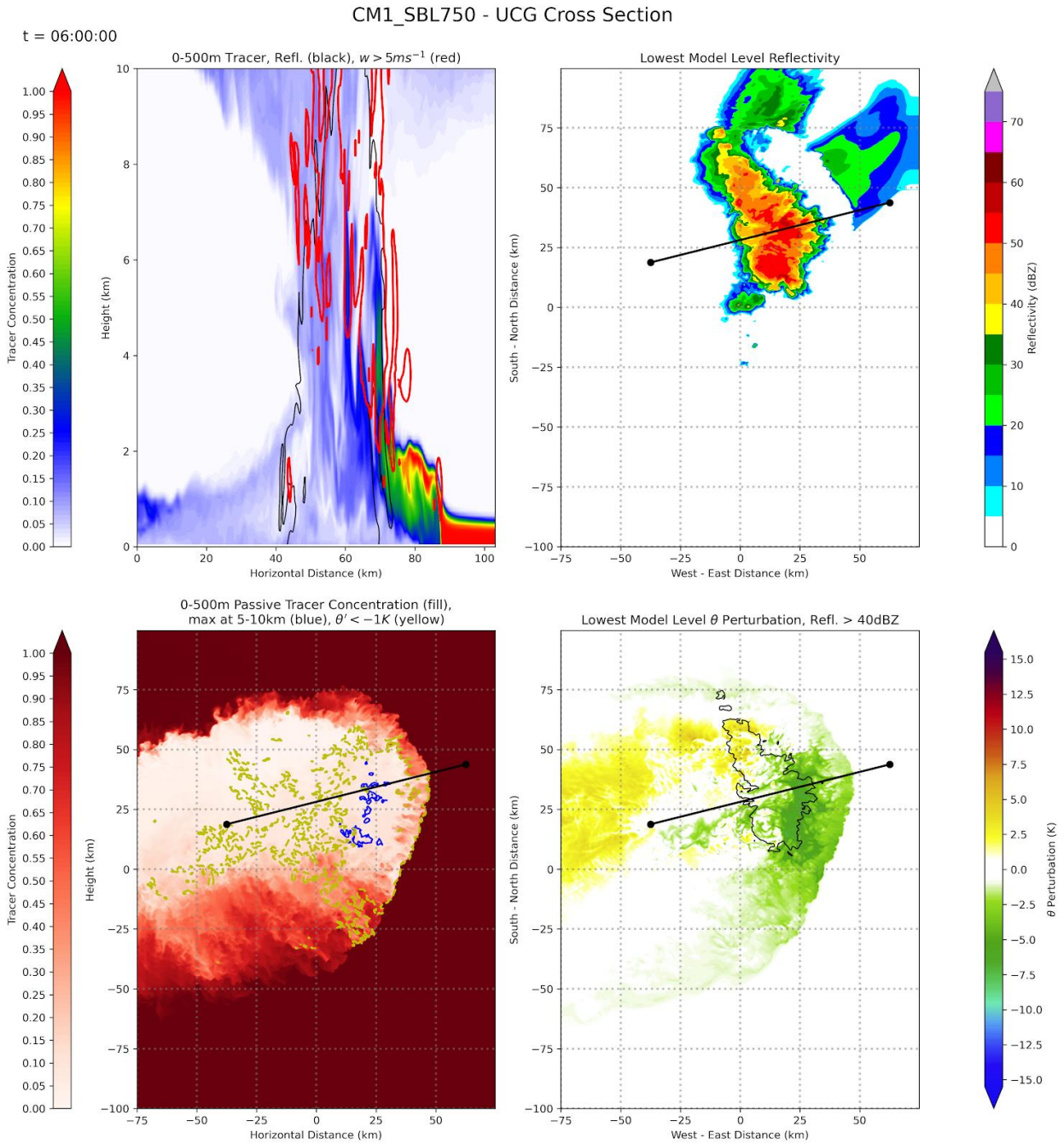

Figure 18: As in Fig. 16, but for the SBL750, UCG experiment at t = 6hr.

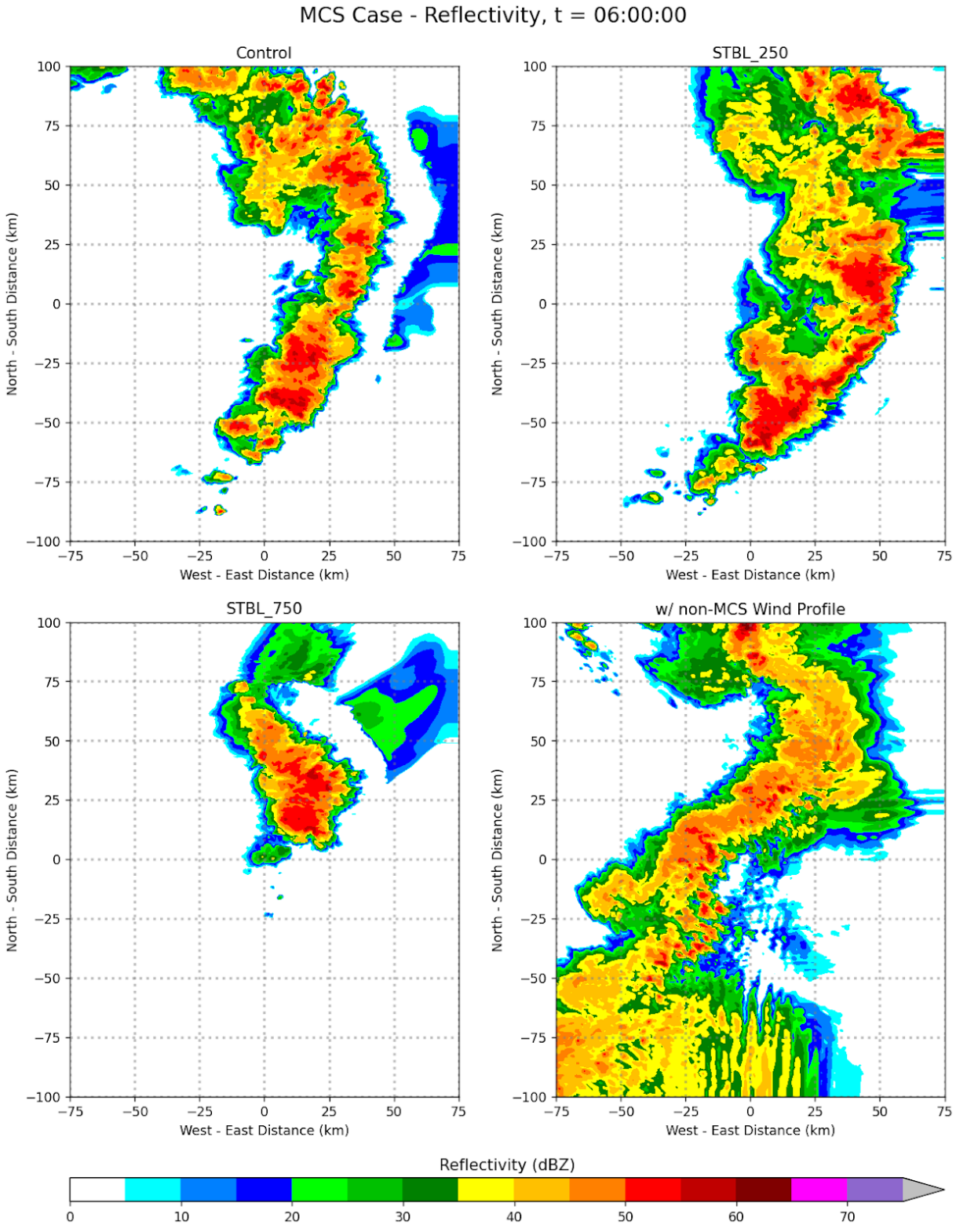

Figure 19: Simulated lowest model level reflectivity for the UCG event in (a) the CTRL, (b) SBL250, (c) SBL750, and (d) WINDR experiments.

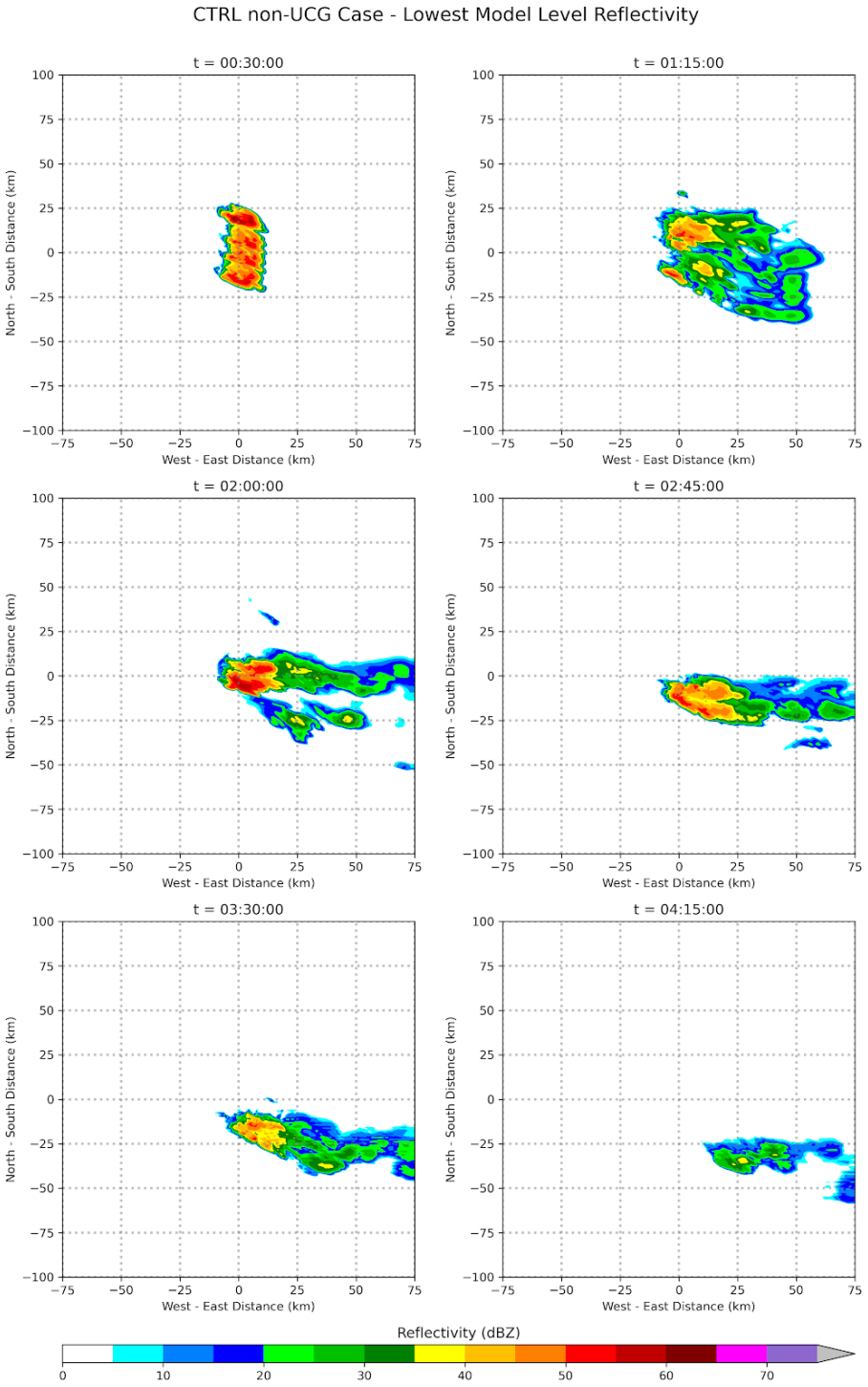

Figure 20: Lowest model level reflectivity for the non-UCG event at (a) 30 minutes, (b) 60 minutes, (c) 90 minutes, and (d) 120 minutes after convective initiation in the CM1.

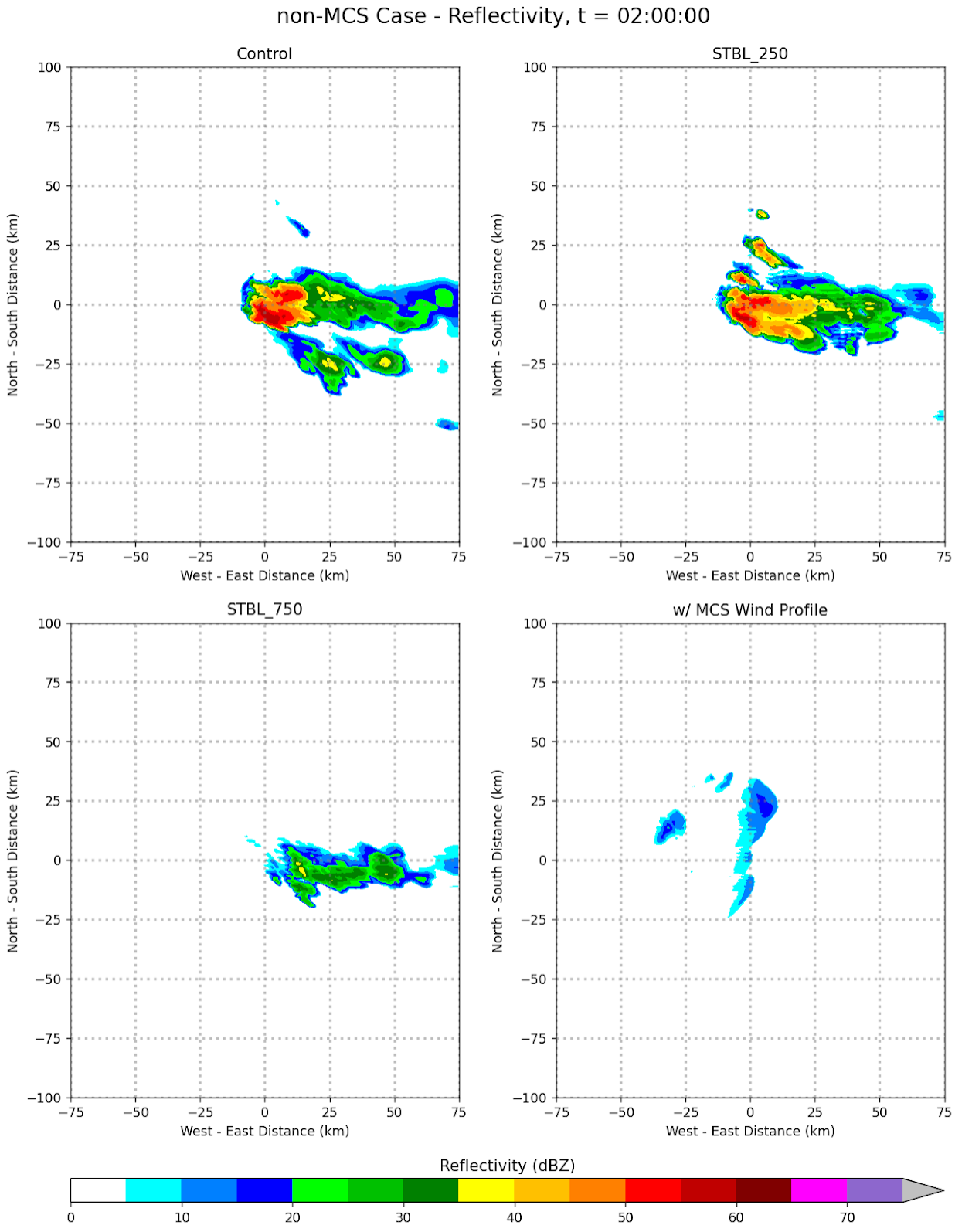

Figure 21: As in Fig. 19, but for the non-UCG event.

CHAPTER 4. GENERAL CONCLUSIONS

4.1 Conclusions

The thesis work presented here explored whether the Weather Research and Forecasting model was capable of discriminating between environments which produce upscale convective growth and those in which cellular convection dominates. It was found that the WRF can do so, with a success rate of 80%. Then, results from each case were aggregated together to test if there were significant differences in cold pool strength and various vertical wind shear magnitudes, which could be used operationally to support severe convection messaging (e.g., Nielsen et al. 2015). However, it was found that outside of the first hour following convective initiation, there were little differences in cold pools strength between cases of UCG and non-UCG. Deep-layer vertical wind shear was found to be statistically significant across all hours and percentile thresholds, which suggests that the ideas of Peters et al. (2017) may be valid, where the authors suggested that deep layer shear is responsible for redistributing hydrometeors to the forward flank, which subsequently organizes the cold pool on the forward flank. Anecdotal evidence of this was found in some WRF simulations, though a thorough investigation was not completed. Low-level wind shear (0-1 km, 0-2.5 km) trends between UCG and non-UCG events showed that shear magnitudes were initially larger in UCG events, though after a few hours this statistically significant difference was no longer observed.

In the cloud-resolving model, the CM1 produced realistic depictions of convection in both UCG and non-UCG events. A shallow stable layer produced very little impact on overall convective evolution, though interestingly a single cell was sustained for far longer in the non-UCG event compared to the CTRL simulation. Adding a 750 m stable layer for both event types also did not change the predominant morphology (e.g., UCG or non-UCG), though it did delay

upscale growth by a few hours in the UCG event. Flipping the wind profiles of the UCG and non-UCG event also did little to impact overall convective morphology, with several convective features maintained (e.g., Fig. 19). Despite the surface stable layer in the SBL250 and SBL750 experiments, a surface based cold pool forms within a few hours of convective initiation, and surface-based passive tracers are contained in the updrafts of convection, confirming Parker et al. (2020)'s findings that surface-based convection can still occur even in the presence of stable layer over night.

Overall, understanding of upscale convective growth remains quite complicated. While the WRF provides a relatively useful sense of the external, synoptic factors that could influence upscale growth (in particular, deep layer shear), higher resolution experiments are needed to properly understand internal factors, such as the role of convectively generated gravity waves or bores. There are still other subtle factors that may play an important role in the organization of MCSs that are not presented here, and future work (described below) should incorporate not only the findings of the present study as well as other data that would be available in real-time, to aid in the eventual prediction of UCG in operational forecast settings.

4.2 Future Work

While this work does extensively detail a large collection of UCG and non-UCG events, the results shown in Chapter 3 provide some interesting future research questions. First, it would be useful to confirm the results of the primary findings here utilizing a WRF setup in which the microphysics, planetary boundary layer physics, and surface layer physics differ from the setup here to confirm the findings that cold pools are not significantly different between UCG and non-UCG events. Squitieri and Gallus (2020) do this to an extent, though their work only focuses on the mature stages of only MCS cases. It is also worth investigating the impact of mid-level (e.g., 700-500hPa) storm relative wind on hydrometeor distribution and cold pool formation. While the

CM1 experiments did flip the wind profiles from a UCG and non-UCG event, modification to deep-layer shear profiles was not performed. Given the robust statistical significance of the deep layer shear from the WRF portion of this work, this is an area of interest that should be explored more in the future.

Finally, there are many other possible experiments that could be performed using the CM1. Using passive tracers, it would be possible to determine the primary source of downdraft air in a variety of thermodynamic profiles. How sensitive is the downdraft region and resultant cold pool to small changes in the temperature and moisture profile (e.g., θ_e)? What is the primary mechanism driving sustained convection and upscale growth in the absence of a surface cold pool? For example, both gravity waves and bores were observed in the CM1, and incorporating both passive parcels and different layers of passive tracers will likely be useful in determining the role of these phenomena.

REFERENCES

Adams-Selin, R. D., S. C. van den Heever, and R. H. Johnson, 2013: Sensitivity of bow-echo simulation to microphysical parameterizations. *Wea. Forecasting*, **28**, 1188-1209, https://doi.org/10.1175/waf-d-12-00108.1.

Blanchard, D. O., 1990: Mesoscale convective patterns of the Southern High Plains. *Bull. Amer. Meteor. Soc.*, **71**, 994-1005, https://doi.org/10.1175/1520-0477(1990)071%3C0994:mcpots%3E2.0.co;2.

Bodine, D. J., and K. L. Rasmussen, 2017: Evolution of mesoscale convective system and organizational structure and convective line propagation. *Mon. Wea. Rev.*, **145**, 3419-3440, https://doi.org/10.1175/mwr-d-16-0406.1.

Borque, P., S. W. Nesbitt, R. J. Trapp, S. Lasher-Trapp, and M. Oue, 2020: Observational study of the thermodynamics and morphological characteristics of a midlatitude continental cold pool event. *Mon. Wea. Rev.*, **148**, 719-737, https://doi.org/10.1175/mwr-d-19-0068.1.

Bryan, G. H., J. M. Fritsch, 2002: A benchmark simulation for moist nonhydrostatic numerical models. *Mon. Wea. Rev.*, **130**, 2917-2928, https://doi.org/10.1175/1520-0493(2002)130%3C2917:absfmn%3E2.0.co;2.

Bryan, G. H., J. C. Wyngaard, and J. Michael Fritsch, 2003: Resolution requirements for the simulation of deep moist convection. *Mon. Wea. Rev.*, **131**, 2394-2416, https://doi.org/10.1175/1520-0493(2003)131%3C2394:rrftso%3E2.0.co;2.

Bryan, G. H., and H. Morrison, 2012: Sensitivity of a simulated squall line to horizontal resolution and parameterization of microphysics. *Mon. Wea. Rev.*, **140**, 202-225, https://doi.org/10.1175/MWR-D-11-00046.1.

Chasteen, M. B., S. E. Koch, and D. B. Parsons, 2019: Multiscale processes enabling the longevity and daytime persistence of a nocturnal mesoscale convective system. *Mon. Wea. Rev.*, **147**, 733-761, https://doi.org/10.1175/mwr-d-18-0233.1.

Clark, A. J., W. A. Gallus, M. Xue, and F. Kong, 2009: A comparison of precipitation forecast skill between small convection-allowing and large convection-parameterizing ensembles. *Wea. Forecasting*, **24**, 1121-1140, https://doi.org/10.1175/2009waf2222222.1.

Clark, A. J., J. S. Kain, P. T. Marsh, J. Correia, M. Xue, and F. Kong, 2012: Forecasting tornado pathlengths using a three-dimensional object identification algorithm applied to convection-allowing forecasts. *Wea. Forecasting*, **27**, 1090-1113, https://doi.org/10.1175/waf-d-11-00147.1.

Coniglio, M. C., J. Y. Hwang, and D. J. Stensrud, 2010: Environmental factors in the upscale growth and longevity of MCSs derived from Rapid Update Cycle analyses. *Mon. Wea. Rev.*, **138**, 3514-3539, https://doi.org/10.1175/2010MWR3233.1.

Coniglio, M. C., S. F. Corfidi, and J. S. Kain, 2011: Environment and early evolution of the 8 May 2009 derecho-producing convective system. *Mon. Wea. Rev.*, **139**, 1083-1102, https://doi.org/10.1175/2010MWR3413.1.

Coniglio, M. C., S. M. Hitchcock, K. H. Knopfmeir, 2016: Impact of assimilating preconvective upsonde observations on short-term forecasts of convection observed during MPEX. *Mon. Wea. Rev.*, **144**, 4301-4325, https://doi.org/10.1175/mwr-d-16-0091.1.

Corfidi, S. F., S. J. Corfidi, and D. M. Schultz, 2008: Elevated convection and castellanus: Ambiguities, significance, and questions. *Wea. Forecasting*, **23**, 1280-1303, https://doi.org/10.1175/2008waf2222118.1.

Dial, G. L., J. P. Racy, and R. L. Thompson, 2010: Short-term convective mode evolution along synoptic boundaries. *Wea. Forecasting*, **25**, 1430-1446, https://doi.org/10.1175/2010waf2222315.1.

Done, J., C. A. Davis, and M. Weisman, 2004: The next generation of NWP: Explicit forecasts of convection using the weather research and forecasting (WRF) model. *Atmos. Sci. Lett.*, **5**, 110-117, https://doi.org/10.1002/asl.72.

Doswell, C. A., 1987: The distinction between large-scale and mesoscale contribution to severe convection: A case study example. *Wea. Forecasting*, **2**, 3-16, https://doi.org/10.1175/1520-0434(1987)002%3C0003:tdblsa%3E2.0.co;2.

Doswell, C. A., H. E. Brooks, and M. P. Kay, 2005: Climatological estimates of daily nontornadic severe thunderstorm probability for the United States. *Wea. Forecasting*, **20**, 577-595, https://doi.org/10.1175/waf866.1.

Droegemeier, K. K., and R. B. Wilhelmson, 1985: Three-dimensional numerical modeling of convection produced by interacting thunderstorm outflows. Part II: Variations in vertical wind shear. *J. Atmos. Sci*., **42**, https://doi.org/10.1175/1520-0469(1985)042%3C2404:tdnmoc%3E2.0.co;2.

Duda, J. D., and W. A. Gallus, 2010: Spring and summer Midwestern severe weather reports in supercells compared to other morphologies. *Wea. Forecasting*, **25**, 190-206, https://doi.org/10.1175/2009waf2222338.1.

Duda, J. D., and W. A. Gallus, 2013: The impact of large-scale forcing on skill of simulated convective initiation and upscale evolution with convection-allowing grid spacings in the WRF*. *Wea. Forecasting*, **28**, 994-1018, https://doi.org/10.1175/waf-d-13-00005.1.

Fowle, M. A., and P. J. Roebber, 2003: Short-range (0-48h) numerical prediction of convective occurrence, mode, and location. *Wea. Forecasting*, **18**, 782-794, https://doi.org/10.1175/1520-0434(2003)018%3C0782:SHNPOC%3E2.0.CO;2.

Fritsch, J. M., R. J. Kane, and C. R. Chelius, 1986: The contribution of mesoscale convective weather systems to the warm-season precipitation in the United States. *J. Clim.*, **25**, 1333-1345, https://doi.org/10.1175/1520-0450(1986)025%3C1333:TCOMCW%3E2.0.CO;2.

Gallo, B. T., and Coauthors, 2017: Breaking new ground in severe weather prediction: The 2015 NOAA/Hazardous weather testbed spring forecasting experiment. *Wea. Forecasting*, **32**, 1541-1568, https://doi.org/10.1175/waf-d-16-0178.1.

Geerts, B., and Coauthors, 2017: The 2015 plains elevated convection at night field project. *Bull. Amer. Meteor. Soc.*, **98**, 767-786, https://doi.org/10.1175/bams-d-15-00257.1.

Grams, J. S., R. L. Thompson, D. V. Snively, J. A. Prentice, G. M. Hodges, and L. J. Reames, 2012: A climatology and comparison of parameters for significant tornado events in the United States. *Wea. Forecasting*, **27**, 106-123, https://doi.org/10.1175/waf-d-11-00008.1.

Grasmick, C., B. Geerts, D. D. Turner, Z. Wang, and T. M. Weckwerth, 2018: The relation between nocturnal MCS evolution and its outflow boundaries in the stable boundary layer: An observational study of the 15 July 2015 MCS in PECAN. *Mon. Wea. Rev.*, **146**, 3203-3226, https://doi.org/10.1175/mwr-d-18-0169.1.

Guyer, J. L., and I. L. Jirak, 2014: The utility of storm-scale ensemble forecasts of cool season severe weather events from the SPC perspective. *27th Conf. on Severe Local Storms*, Madison, WI, Amer. Meteor. Soc., 37, https://ams.confex.com/ams/27SLS/webprogram/Paper254640.html.

Haghi, K. R., B. Geerts, H. G. Chipilski, A. Johnson, D. Degelia, D. Imy, D. B. Parsons, R. D. Adams-Selin, D. D. Turner, and X. Wang, 2019: Bore-ing into nocturnal convection. *Bull. Amer. Meteor. Soc.*, **100**, 1103-1121, https://doi.org/10.1175/bams-d-17-0250.1.

Hawblitzel, D. P., F. Zhang, Z. Meng, and C. A. Davis, 2007: Probabilistic evaluation of the dynamics and predictability of the mesoscale convective vortex of 10-13 June 2003. *Mon. Wea. Rev.*, **135**, 1544-1563, https://doi.org/10.1175/mwr3346.1.

Hitchcock, S. M., M. C. Coniglio, and K. H. Knopfmeier, 2016: Impact of MPEX upsonde observations on ensemble analyses and forecasts of the 31 May 2013 convective event over Oklahoma. *Mon. Wea. Rev.*, **144**, 2889-2913, https://doi.org/10.1175/mwr-d-15-0344.1.

Hitchcock, S. M., R. S. Schumacher, G. R. Herman, M. C. Coniglio, M. D. Parker, and C. L. Ziegler, 2019: Evolution of pre- and postconvective environmental profiles from mesoscale convective systems during PECAN. *Mon. Wea. Rev.*, **147**, 2329-2354, https://doi.org/10.1175/mwr-d-18-0231.1.

Horgan, K. L., D. M. Schultz, J. E. Hales, S. F. Corfidi, and R. H. Johns, 2007: A five-year climatology of elevated severe convective storms in the United States east of the Rocky Mountains. *Wea. Forecasting*, **22**, 1031-1044, https://doi.org/10.1175/waf1032.1.

James, R. P., J. M. Fritsch, and P. M. Markowski, 2005: Environmental distinctions between cellular and slabular convective lines. *Mon. Wea. Rev.*, **133**, 2669-2691, https://doi.org/10.1175/mwr3002.1.

James, R. P., P. M. Markowski, and J. M. Fritsch, 2006: Bow echo sensitivity to ambient moisture and cold pool strength. *Mon. Wea. Rev.*, https://doi.org/10.1175/mwr3109.1.

Jirak, I. L., and W. R. Cotton, 2007: Observational analysis of the predictability of mesoscale convective systems. *Wea. Forecasting*, **22**, 813-838, https://doi.org/10.1175/waf1012.1.

Loveless, D. M., T. J. Wagner, D. D. Turner, S. A. Ackerman, and W. F. Feltz, 2019: A composite perspective on bore passages during the PECAN campaign. *Mon. Wea. Rev.*, **147**, 1395-1413, https://doi.org/10.1175/mwr-d-18-0291.1.

Maddox, R. A., 1980: Mesoscale convective complexes. Bull. Amer. Meteor. Soc., 61, 1374-1387, https://doi.org/10.1175/1520-0477(1980)061%3C1374:mcc%3E2.0.co;2.

Mallinson, H. M., and S. G. Lasher-Trapp, 2019: An investigation of hydrometeor latent cooling upon convective cold pool formation, sustainment, and properties. *Mon. Wea. Rev.*, **147**, 3205-3222, https://doi.org/10.1175/mwr-d-18-0382.1.

Marsham, J. H., S. B. Trier, T. M. Weckwerth, and J. W. Wilson, 2011: Observations of elevated convection initiation leading to a surface-based squall line during 13 June IHOP_2002. *Mon. Wea. Rev.*, **139**, 247-271, https://doi.org/10.1175/2010mwr3422.1.

McAnelly, R. L., J. E. Nachamkin, W. R. Cotton, and M. E. Nicholls, 1997: Upscale evolution of MCSs: Doppler radar analysis and analytical investigation. *Mon. Wea. Rev.*, **125**, 1083-1110, https://doi.org/10.1175/1520-0493(1997)125%3C1083:ueomdr%3E2.0.co;2.

Mulholland, J. P., S. W. Nesbitt, and R. J. Trapp, 2019: A case study of terrain influences on upscale convective growth of a supercell. *Mon. Wea. Rev.*, **147**, 4305-4324, https://doi.org/10.1175/mwr-d-19-0099.1.

Nielsen, E. R., G. R. Herman, R. C. Tournay, J. M. Peters, and R. S. Schumacher, 2015: Double impact: When both tornadoes and flash floods threaten the same place at the same time. *Wea. Forecasting*, **30**, 1673-1693, https://doi.org/10.1175/waf-d-15-0084.1.

Parker, M. D., 2018: External vs. self-organization of nocturnal MCSs from PECAN. *29th Conf. on Severe Local Storms*, Stowe, VT, Amer. Meteor. Soc., 4.5, https://ams.confex.com/ams/29SLS/meetingapp.cgi/Paper/348312.

Parker, M. D., B. S. Borchardt, R. L. Miller, and C. L. Ziegler, 2020: Simulated evolution and severe wind production by the 25-26 June 2015 nocturnal MCS from PECAN. *Mon. Wea. Rev.*, **148**, 183-209, https://doi.org/10.1175/mwr-d-19-0072.1.

Parsons, D. B., K. R. Haghi, K. T. Halbert, B. Elmer, and J. Wang, 2019: The potential role of atmospheric bores and gravity waves in the initiation and maintenance of nocturnal convection over the Southern Great Plains. *J. Atmos. Sci.*, **76**, 43-68, https://doi.org/10.1175/jas-d-17-0172.1.

Peters, J. M., and R. S. Schumacher, 2015: The simulated structure and evolution of a quasi-idealized warm-season convective system with a training convective line. *J. Atmos. Sci.*, **72**, 1987-2010, https://doi.org/10.1175/jas-d-14-0215.1.

Peters, J. M., and R. S. Schumacher, 2016: Dynamics governing a simulated mesoscale convective system with a training convective line. J. Atmos. Sci., 73, 2643-2664, https://doi.org/10.1175/jas-d-15-0199.1.

Peters, J. M., K. C. Eure, and R. S. Schumacher, 2017: Factors that drive MCS growth from supercells. *17th Conf. on Mesoscale Processes*, San Diego, CA, Amer. Meteor. Soc., 9.6, https://ams.confex.com/ams/17MESO/webprogram/Paper320248.html.

Rotunno, R., J. B. Klemp, and M. L. Weisman, 1988: A theory for strong, long-lived squall lines. *J. Atmos. Sci.*, **45**, 463-485, https://doi.org/10.1175/1520-0469(1988)045%3C0463:atfsll%3E2.0.co;2.

Schumacher, R. S., 2015: Resolution dependence of initiation and upscale growth of deep convection in convection-allowing forecasts of the 31 May-1 June 2013 supercell and MCS. *Mon. Wea. Rev.*, **143**, 4331-4354, https://doi.org/10.1175/mwr-d-15-0179.1.

Schwartz, C. S., and Coauthors, 2009: Next-day convection-allowing WRF model guidance: A second look at 2-km versus 4-km grid spacing. *Mon. Wea. Rev.*, **137**, 3351-3372, https://doi.org/10.1175/2009mwr2924.1.

Skamarock, W. C., and Coauthors, 2019: A description of the advanced research WRF version 4. *NCAR Tech. Note NCAR/TN-556+STR*, 145pp. https://doi.org/10.5065/1dfh-6p97.

Smith, B. T., R. L. Thompson, J. S. Grams, C. Broyles, and H. E. Brooks, 2012: Convective modes for significant severe thunderstorms in the contiguous United States. Part I: Storm classification and climatology. *Wea. Forecasting*, **27**, 1114-1135, https://doi.org/10.1175/waf-d-11-00115.1.

Squitieri, B. J., and W. A. Gallus, 2020: On the forecast sensitivity of MCS cold pools and related features to horizontal grid spacing in convection-allowing WRF simulations. *Wea. Forecasting*, **35**, 325-346, https://doi.org/10.1175/waf-d-19-0016.1.

Szoke, E. J., J. Brown, and B. Shaw, 2004: Examination of the performance of several mesoscale models for convective forecasting during IHOP. Preprints, *20th Conf. on Weather Analysis and Forecasting*, Seattle, WA, Amer. Meteor. Soc., J13.6. [Available online at https://ams.confex.com/ams/pdfpapers/68930.pdf.]

Thielen, J. E., and W. A. Gallus, 2019: Influences of horizontal grid spacing and microphysics on WRF forecasts of convective morphology evolution for nocturnal MCSs in weakly forced environments. *Wea. Forecasting*, **34**, 1495-1517, https://doi.org/10.1175/waf-d-18-0210.1.

Thompson, R. L., R. Edwards, J. A. Hart, K. L. Elmore, and P. Markowski, 2003: Close proximity soundings within supercell environments obtained from the Rapid Update Cycle. *Wea. Forecasting*, **18**, 1243-1261, https://doi.org/10.1175/1520-0434(2003)018%3C1243:cpswse%3E2.0.co;2.

Thompson, R. L., B. T. Smith, J. S. Grams, A. R. Dean, and C. Broyles, 2012: Convective modes for significant severe thunderstorms in the contiguous United States. Part II: Supercell and QLCS tornado environments, https://doi.org/10.1175/WAF-D-11-00116.1.

Weisman, M. L., 1992: The role of convectively generated rear-inflow jets in the evolution of long-lived mesoconvective systems. *J. Atmos. Sci*., **49**, 1826-1847, https://doi.org/10.1175/1520-0469(1992)049%3C1826:trocgr%3E2.0.co;2.

Weisman, M. L., W. C. Skamarock, and J. B. Klemp, 1997: The resolution dependence of explicitly modeled convective systems. *Mon. Wea. Rev*., **125**, 527-548 https://doi.org/10.1175/1520-0493(1997)125%3C0527:trdoem%3E2.0.co;2.

Weisman, M. L., and R. Rotunno, 2004: "A theory for strong long-lived squall lines" revisited. *J. Atmos. Sci.*, **61**, 361-382, https://doi.org/10.1175/1520-0469(2004)061%3C0361:atfsls%3E2.0.co;2.

Weisman, M. L., C. Davis, W. Wang, K. W. Manning, and J. B. Klemp, 2008: Experiences with 0-36-h explicit convective forecasts with the WRF-ARW model. *Wea. Forecasting*, **23**, 407-437, https://doi.org/10.1175/2007WAF2007005.1.

Weisman, M. L., and Coauthors, 2015: The mesoscale predictability experiment (MPEX). *Bull. Amer. Meteor. Soc.*, **96**, 2127-2149, https://doi.org/10.1175/bams-d-13-00281.1.

Weiss, S. J., M. E. Pyle, Z. Janjic, D. R. Bright, and G. J. DiMego, 2008: The operational high resolution window WRF model runs at NCEP: Advantages of multiple model runs for severe convective weather forecasting. *24th Conf. on Severe Local Storms*, Savannah, GA, Amer. Meteor. Soc., P10.8, https://ams.confex.com/ams/pdfpapers/142192.pdf.

Wilson, J. W., and R. D. Roberts, 2006: Summary of convective storm initiation and evolution during IHOP: Observational and modeling perspective. *Mon. Wea. Rev*., **134**, 23–47, https://doi.org/10.1175/mwr3069.1.

Zhang, S., D. B. Parsons, and Y. Wang, 2020: Wave disturbances and their role in the maintenance, structure, and evolution of a mesoscale convection system. *J. Atmos. Sci.*, **77**, 51-77, https://doi.org/10.1175/jas-d-18-0348.1.